THE PERMANENT DEFORMATION OF STEEL PORTAL FRAMES SUBJECTED TO IMPULSIVE LOADING

by

D. Hanan

A thesis submitted in partial fulfilment
of the requirements for the degree of
Master of Science in Engineering

Department of Civil Engineering
University of Cape Town

September 1977

The copyright of this thesis vests in the author. No quotation from it or information derived from it is to be published without full acknowledgement of the source. The thesis is to be used for private study or non-commercial research purposes only.

Published by the University of Cape Town (UCT) in terms of the non-exclusive license granted to UCT by the author.

University of Cape Town

To the memory of Vera

DECLARATION OF CANDIDATE

I, Davide Hanan, hereby declare that this thesis is my own work and that it has not been submitted for a degree at another university.

Signed by candidate Signature Removed

. . . . . .

September 1977

LIST OF CONTENTS

ACKNOWLEDGEMENTS

I wish to express my gratitude to Professor J.B. Martin for his supervision and assistance throughout the thesis.

I am indebted to the Council for Scientific and Industrial Research for financial assistance during this project.

Thanks are also due to the many other people who made this project possible:

Professor P.S. Symonds and C.T. Chon for sending an interim copy of their paper,

Giles Pearson for designing and manufacturing the velocity transducer and its calibrating device,

Mr Beverton and the staff of the Civil Engineering Department workshop for their cooperation with the experimental work,

The staff of the Central Accoustics Laboratory (UCT) and

Dr Naude of the National Institute of Metallurgy (UCT) for their advice on experimental techniques and for lending valuable equipment on numerous occasions,

Lee Behm for typing the manuscript, and Harold Cable for reproducing copies of the thesis.

ABSTRACT

The inelastic response of steel portal frames with a mass attached to the centre of the beam member and subjected to large dynamic loads is studied. The analysis is carried out using the mode approximation technique extended to include strain-rate sensitivity, finite deflections and pulse duration. Experimental results are presented which show good agreement with theoretical predictions. The use of the extended Hamilton's principle for mode form solutions is discussed.

INTRODUCTION

The treatment of inelastic dynamic loading problems in structures has been achieved along two distinct lines: the numerical approach and the more traditional analytical approach.

Simple analytical methods are extremely useful for preliminary stages of design and may even be adequate for the final design in many cases. They further provide insight into the mechanics of the deformation process, covering a wide class of problems. In those cases where the external dynamic loads can be accurately determined, or when theoretical methods are not available, the numerical methods [1, 2] may be used. These are however long and complex, and it is desirable to have simple approximate methods.

Of interest here is the mode approximation technique developed by Martin and Symonds [3] for rigid-plastic structures loaded impulsively. This technique has been extended to more general inelastic behaviour. Symonds [4] used the technique as a starting point for an approximate theory including strain rate and strain hardening effects. Lee and Martin [5], Lee [6] and Symonds [7] discussed mode approximation concepts for viscous and rigid-viscoplastic materials. An analogous technique for the case of load pulses of finite duration was further developed by Augusti, Martin and O'Keeffe [8]. Apart from simple beams, very few structures composed of straight bars have been studied.

It is the purpose of this thesis to investigate the mode approximation technique applied to the analysis of mild steel portal frames (rectangular and trapezoidal) subjected to impulse loading at the centre of the beam. This class of structures has many advantages as an object of study since they are widely used in engineering practice and are nevertheless sufficiently simple so that both analysis and experiments are fairly simple to carry out and compare. Most of the previous work on the analysis of portal frames was based on two degree of freedom models (Rawlings [9]) or on the mode solution where strain rate effects were included by correcting the yield moment (Perrone [10], Martin and Johnson [11]). Fully numerical methods have also been used by Johnson, Al-Hassani and Hashmi [1]. Symonds and Chon [25] have recently used a method similar to the one described here.

In the present analysis, the mode approximation technique is extended to include strain rate effects, geometry changes and pulse duration. Elastic effects are ignored. This assumption, as pointed out by Symonds [12] is only valid if the applied kinetic energy is considerably larger than the maximum amount of strain energy which can be absorbed in a wholly elastic manner. It is also important that the duration of loading be short compared to the natural period of elastic vibration.

An experimental program designed to test the validity of the analysis is reported. Results are presented which show reasonable agreement with theoretical predictions. The energy ratio for the test performed varied between 3 and 13. Transient responses were recorded with a velocity transducer.

The use of the extended Hamilton's principle [13] for mode form solutions is also discussed. It is shown that Martin and Lee's extremum principle [5] may be derived from it.

PART I: ANALYTICAL STUDY

1. The constitutive equation

The dependence of the dynamic lower yield stress $\sigma(\dot{\varepsilon})$ on the plastic strain rate $\dot{\varepsilon}$ has been represented in numerical form [14] by

$$\frac{\sigma(\dot{\varepsilon})}{\sigma_o} = 1 + \left(\frac{\dot{\varepsilon}}{\dot{\varepsilon}_o}\right)^{\frac{1}{n}} \qquad \text{for } |\sigma| \geq \sigma_o, \tag{1.1}$$

where σ_o is the yield stress, as derived from tests at various strain rates rather than the usual static test; $\dot{\varepsilon}_o$ and n are material constants. This formula (with $n = 5$, $\dot{\varepsilon}_o = 40\text{sec}^{-1}$) represents satisfactorily the tension impact tests of Manjoine [15] and the tests in pure bending of Aspden and Campbell [16]. It implies that the material is of rigid-viscoplastic type: no deformation occurs if $|\sigma| < \sigma_o$.

The inhomogeneity of this constitutive relation makes for major difficulties in the analysis of dynamic problems. The mode approximation technique is substantially simplified if the constitutive equation is homogeneous; permanent mode solutions then exist, for example. For that purpose, Symonds [7] made use of the concept of a 'matched viscous' representation, in which equation (1.1) is replaced by

$$\frac{\sigma}{\sigma'_o} = \left(\frac{\dot{\varepsilon}}{\dot{\varepsilon}_o} \right)^{\frac{1}{n'}} . \qquad (1.2)$$

Since microscopic models of slip dynamics, as well as modern developments in constitutive laws define plastic strain rate as occurring at all stress levels, the homogeneous viscous representation which has this property may be regarded as no less suitable for plastic structural dynamics than the customary rigid-viscoplastic representation [7].

If the rigid-viscoplastic type of law (1.1) is regarded as correct, it is possible to match equation (1.2) to it in various ways. Symonds [7] chose σ'_o and n' in terms of σ_o and n in such a way that the error remained conservative in the sense that the actual material is replaced by a weaker one. He ensured this by making the curve $\sigma = \sigma(\dot{\varepsilon})$ of equation (1.2) touch that of equation (1.1) with a common tangent at a particular strain rate $\dot{\varepsilon}^*$. This implies that different curves are used for different problems or the same problem with varied loading conditions. It is felt here that this is not necessary in view of the fact that equation (1.1) is itself an approximation. It is thus proposed to match (1.2) to (1.1) by a single curve, using the least square error method.

Figure 1.1 shows the rigid-viscoplastic and viscous curves.

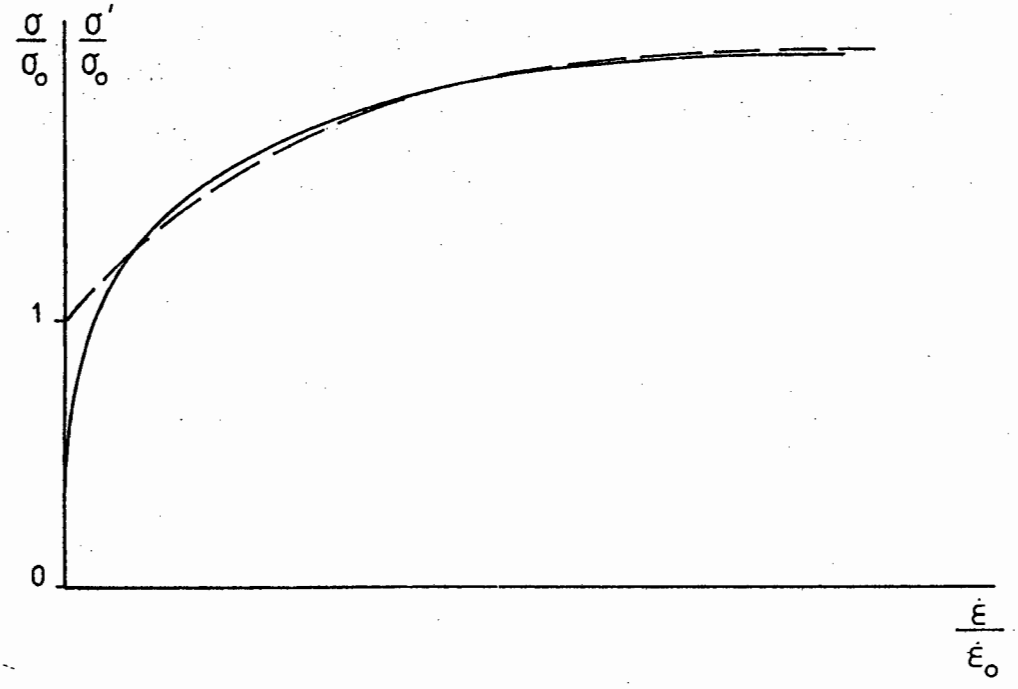

Figure 1.1

From (1.1) and (1.2) we have

$$\frac{\sigma}{\sigma_o} = 1 + \left(\frac{\dot{\varepsilon}}{\dot{\varepsilon}_o}\right)^{\frac{1}{5}},$$

$$\frac{\sigma'}{\sigma_o} = \mu \left(\frac{\dot{\varepsilon}}{\dot{\varepsilon}_o}\right)^{\alpha},$$

where $\mu = \frac{\sigma'_o}{\sigma_o}$ and $\alpha = \frac{1}{n'}$.

The error at any value of $\frac{\dot{\varepsilon}}{\dot{\varepsilon}_o}$ is given by

$$\frac{\sigma}{\sigma_o} - \frac{\sigma'}{\sigma_o} = 1 + \left(\frac{\dot{\varepsilon}}{\dot{\varepsilon}_o}\right)^{\frac{1}{5}} - \mu\left(\frac{\dot{\varepsilon}}{\dot{\varepsilon}_o}\right)^{\alpha}.$$

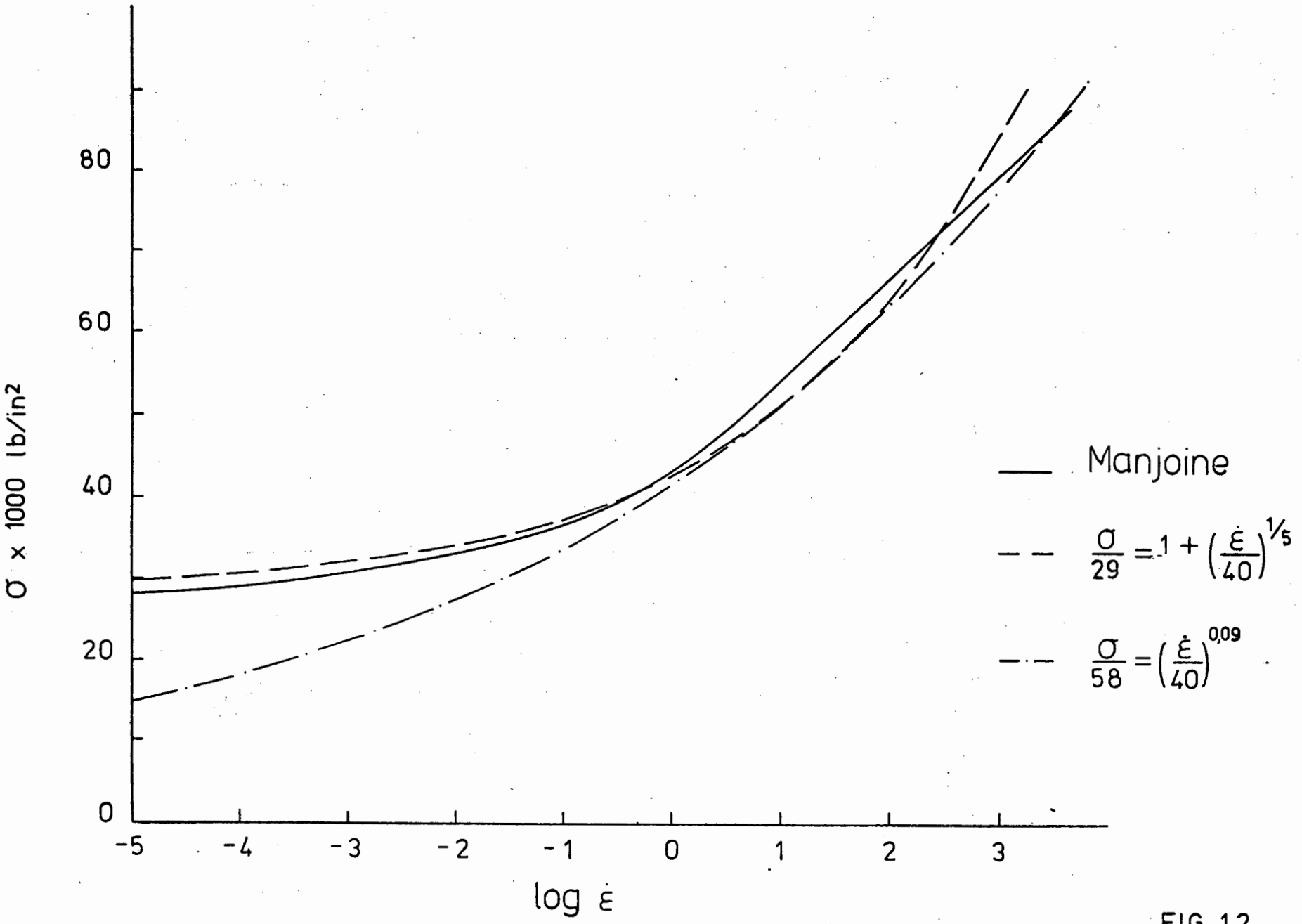
80
60
40
20
0
σ x 1000 lb/in²
-5
-4
-3
-2
-1
0
1
2
3
log ε̇
Manjoine
σ/29 = 1 + (ε̇/40)^1/5
σ/58 = (ε̇/40)^0,09

FIG. 1.2

This is squared and integrated over the interval $0 \leq \frac{\dot{\varepsilon}}{\dot{\varepsilon}_o} \leq A$:

$$S = \int_0^A \left(\frac{\sigma}{\sigma_o} - \frac{\sigma'}{\sigma_o} \right)^2 d\left(\frac{\dot{\varepsilon}}{\dot{\varepsilon}_o} \right) = A + \frac{5A^{\frac{6}{5}}}{3} - \frac{2\mu A^{(\alpha+1)}}{\alpha + 1} + \frac{5A^{\frac{7}{5}}}{7} + \frac{\mu^2 A^{(2\alpha+1)}}{2\alpha + 1} - \frac{2\mu A^{(\alpha+\frac{6}{5})}}{\alpha + \frac{6}{5}}$$

S is then minimized. For A = 2 (range of interest in this study - see Part II), we get $\mu = 2$ and $\alpha = 0{,}09$ i.e. (1.2) becomes

$$\frac{\sigma}{2\sigma_o} = \left(\frac{\dot{\varepsilon}}{\dot{\varepsilon}_o} \right)^{0{,}09} = \left(\frac{\dot{\varepsilon}}{\dot{\varepsilon}_o} \right)^{\frac{1}{11{,}111}} . \qquad (1.3)$$

Figure 1.2 shows a comparison between the rigid-viscoplastic curve, the viscous curve and Manjoine's experimental curve for which $\sigma_o = 29$ kip, $\dot{\varepsilon}_o = 40$ and $n = 5$. It can be seen that the viscous curve is everywhere below Manjoine's curve for rates less than 10^3 and the error induced is thus still conservative.

2. The use of Hamilton's principle for mode form solutions

A number of variational principles have been formulated to obtain mode solutions of a structure deforming plastically as a result of dynamic loading (see for example Lee and Martin [5]; Lee [6]; Martin [17]; Symonds and Wierzbicki [18]). Taya and Mura [13] have recently used an extended Hamilton's principle to analyse rigid-plastic structures. We shall here further extend

Hamilton's principle to include viscous materials and show how Lee and Martin's minimum principle may be derived from it.

For this purpose we treat bar structures composed of viscous material where the bending moment M and the curvature rate $\dot{\kappa}$ are the only generalized stress and strain. The constitutive relation is thus

$$\frac{M}{M_o} = \left(\frac{\dot{\kappa}}{\dot{\kappa}_o} \right)^{\frac{1}{n}}, \tag{2.1}$$

where M_o and $\dot{\kappa}_o$ are constants.

The structure occupies a domain S; loads p(s,t) are specified on part S_T, while velocities $\dot{u} = 0$ everywhere on S_u. The displacement and acceleration are represented by u and $\ddot{u}$ respectively. Consider the identity

$$\frac{d}{dt} \dot{u}\delta u = \ddot{u}\delta u + \dot{u}\delta\dot{u}. \tag{2.2}$$

Multiply both sides by m and integrate over the domain S:

$$\frac{d}{dt} \int_S m\dot{u}\delta u\,ds = \int_S m\ddot{u}\delta u\,ds + \int_S m\dot{u}\delta\dot{u}\,ds. \tag{2.3}$$

The principle of virtual work gives

$$\int_S P\delta u\,ds - \int_S M\delta\kappa\,ds = \int_S m\ddot{u}\delta u\,ds \tag{2.4}$$

From (2.3) and (2.4) we get

$$\frac{d}{dt}\int_S m\dot{u}\delta u\,ds = \int_S P\delta u\,ds - \int_S M\delta\kappa\,ds + \int_S m\dot{u}\delta\dot{u}\,ds \qquad (2.5)$$

Integrate both sides over the time interval $[t_1, t_2]$:

$$\int_S m\dot{u}\delta u\,ds\Big]_{t_1}^{t_2} = \int_{t_1}^{t_2}\Big(\int_S P\delta u\,ds - \int_S M\delta\kappa\,ds + \int_S m\dot{u}\delta\dot{u}\,ds\Big)\,dt. \qquad (2.6)$$

If we select $\delta u(t_1) = \delta u(t_2) = 0$, (2.6) becomes

$$\int_{t_1}^{t_2}\Big(\int_S P\delta u\,ds - \int_S M\delta\kappa\,ds + \int_S m\dot{u}\delta\dot{u}\,ds\Big)\,dt = 0 \qquad (2.7)$$

Let T = kinetic energy $= \int_S \frac{1}{2} m\dot{u}^2 ds$,

W = potential of external loads $= \int_S Pu\,ds$.

Then

$$\delta T = \int_S m\dot{u}\delta\dot{u}\,ds,$$

and

$$\delta W = \int_S P\delta u\,ds.$$

Equation (2.7) becomes

$$\int_{t_1}^{t_2}(\delta W + \delta T)dt = \int_{t_1}^{t_2}\int_S M\delta\kappa ds dt. \tag{2.8}$$

This is in fact Hamilton's principle (see for example [26]) from which the equation of motion may be derived. Equation (2.7) may be written as

$$\int_{t_1}^{t_2}\int_S (m\dot{u}\delta\dot{u} + P\delta u - M\delta u_{xx})ds\, dt = 0 \tag{2.9}$$

We wish to find an expression dependant on δu only. The first and third terms of (2.9) may be integrated by parts:

$$\int_{t_1}^{t_2}\int_S m\dot{u}\delta\dot{u}ds dt = \int_S m\dot{u}\delta u ds\Big]_{t_1}^{t_2} - \int_{t_1}^{t_2}\int_S m\ddot{u}\delta u ds dt,$$

$$= -\int_{t_1}^{t_2}\int_S m\ddot{u}\delta u ds dt, \tag{2.10}$$

and

$$\int_S M\delta u_{xx} ds = M\delta u_x\Big]_S - \int_S M_x\delta u_x ds,$$

$$= M\delta u_x\Big]_S - M_x\delta u\Big]_S + \int_S M_{xx}\delta u ds,$$

$$= \int_S M_{xx}\delta u ds. \tag{2.11}$$

The first two terms disappear since the varied path must satisfy the boundary conditions at any instant.

Substituting (2.10) and (2.11) in (2.9):

$$\int_{t_1}^{t_2} \int_S (-m\ddot{u} - \frac{d^2M}{dx^2} + P)\,\delta u ds dt = 0, \tag{2.12}$$

i.e.

$$\frac{d^2M}{dx^2} + m\ddot{u} = P, \tag{2.13}$$

which is the differential equation governing the motion of a beam element.

When the moment M is constant, as in the rigid-plastic case, equation (2.8) may be written as

$$\int_{t_1}^{t_2} (\delta W + \delta T)dt = \int_{t_1}^{t_2} \delta E dt,$$

where

$$E = \int_S M\kappa ds$$

This is the extended Hamilton's principle as proposed by Taya and Mura [13], in which E is the dissipated energy.

For viscous materials, M is not a constant and (2.14) does not hold. A similar equation may however be derived if we define $\dot{u}$ to be of mode form:

$$\dot{u} = v^*\phi(x)T(t). \tag{2.15}$$

i.e.

$$\dot{\kappa} = v^* \phi_{xx}(x)T(t), \tag{2.16}$$

$$\kappa = v^* \phi_{xx} \int T dt = v^* \phi_{xx} T^*. \tag{2.17}$$

(2.1) becomes

$$M = \frac{M_o}{\dot{\kappa}_o^{1/n}} \left(\frac{T}{T^*} \right)^{\frac{1}{n}} \kappa^{\frac{1}{n}} \tag{2.18}$$

The first variation of E is now

$$\delta E = \int_S \frac{\partial(M\kappa)}{\partial \kappa} \delta\kappa ds,$$

$$= \int_S \left\{ \kappa \frac{\partial M}{\partial \kappa} + M \right\} \delta\kappa ds.$$

Using (2.18), this gives

$$\delta E = \frac{n+1}{n} \int_S M \delta\kappa ds \tag{2.19}$$

Equation (2.7) now reduces to

$$\int_{t_1}^{t_2} (\delta W + \delta T) dt = \frac{n}{n+1} \int_{t_1}^{t_2} \delta E dt. \tag{2.20}$$

where $E = \int_S M\kappa ds$. It must be noted that this is not the dissipated energy.

We shall now show that Martin and Lee's minimum principle [5] can be derived from (2.20). This minimum principle applies to the impulse loading problem: $p(s,t) = 0$. Equation (2.20) becomes:

$$\delta \int_o^{t_f} \int_S \left(\frac{1}{2} m\dot{u}^2 - \frac{n}{n+1} M\kappa\right) ds dt = 0 \qquad (2.21)$$

We seek mode solutions. Substituting (2.15) and (2.17) in (2.20)

$$\delta\Big\{ \frac{mv^{*2}}{2} \int_o^{t_f} T^2 dt \int_S \phi^2 ds$$

$$- \frac{M_o v^{*\frac{n+1}{n}}}{\dot{\kappa}_o^{1/n}} \frac{n+1}{n} \int_o^{t_f} T^{\frac{1}{n}} T^* \, dt \int_S \phi_{xx}^{\frac{n+1}{n}} ds \Big\} = 0 \qquad (2.22)$$

Let

$$A = \int_o^{t_f} T^2 dt,$$

$$B = -\frac{n+1}{n} \int_o^{t_f} T^{\frac{1}{n}} T^* \, dt.$$

Then,

$$\delta\{ A \frac{mv^{*2}}{2} \int_S \phi^2 dx + B \frac{M_o v^{*\frac{n+1}{n}}}{\dot{k}_o^{1/n}} \int_S \phi_{xx}^{\frac{n+1}{n}} ds \} = 0 ,$$

i.e.

$$\delta \{ A \int_S \frac{1}{2} m\dot{u}^2 ds + B \int_S M\dot{\kappa} ds \} = 0,$$

where

$$\dot{u} = v^* \phi(x) ,$$

i.e. $$\delta \{ \int_S M\dot{\kappa} ds + \frac{B}{A} \int_S \frac{1}{2} m\dot{u}^2 ds \} = 0. \qquad (2.23)$$

If $\frac{B}{A}$ is treated as a Lagrangian multiplier, equation (2.22) means that the mode solution $\dot{u}$ makes

$$\int_S M\dot{\kappa} ds$$

stationary subject to the condition

$$\int_S \frac{1}{2} m\dot{u}^2 ds = \text{constant}$$

This is the extremum principle formulated by Lee and Martin [5].

3. Impulsively loaded portal frames

Consider the portal frame shown in Figure 3.1: a trapezoidal frame is treated here for generality; very minor changes are required for rectangular frames.

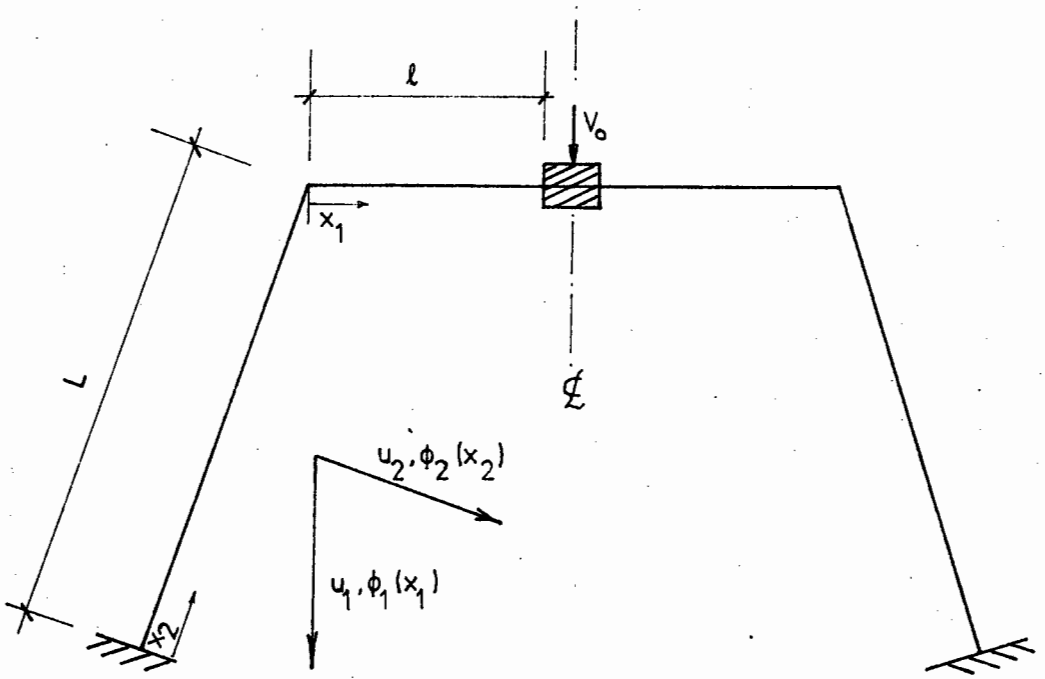

Figure 3.1

The frame is of rectangular cross-section (width b, thickness h), mass m per unit length. A mass G is attached at mid-span, and (treated as a particle) is subjected to an impulse so that its velocity at time t = 0 is V_o. Let $\dot{u}(x_1,t)$, $\dot{u}_2(x_2,t)$ represent the velocities at time t of a point x_i of the beam and column members respectively. The bending moment M and the curvature rate $\dot{\kappa}$ are considered as the only generalized stress and strain. The constitutive equation is thus

$$\frac{M}{M_o} = \left(\frac{\dot{\kappa}}{\dot{\kappa}_o} \right)^{\frac{1}{n}} \tag{3.1}$$

where $M_o = (\mu\sigma_o bh^2)/4$ is the yield moment;

$\dot{\kappa}_o = \frac{2\dot{\varepsilon}_o}{h}(1 + \frac{1}{2n})^n$ is the material rate sensitivity constant for bending curvature rate [5].

Because of the geometrical and loading symmetry, only half of the frame is analysed.

3.1 Small deflection analysis

We seek a mode form approximate solution and write this as

$$\dot{u}_i(x_i,t) = v^*\phi_i(x_i)T(t), \quad i = 1,2 \tag{3.2}$$

where the shape function $\phi_1(x_1)$ is normalised so that $\phi_1(\ell) = 1$, and the time function $T(t)$ is defined so that $T(0) = 1$ and $T(t) = 0$. Thus v^* is the initial velocity at $x_1 = \ell$. The boundary conditions to be satisfied by the mode functions are

$$\dot{u}_1(0,t) = \dot{u}_2(0,t) = \dot{u}_{1x}(\ell,t) = \dot{u}_{2x}(0,t) ,$$

$$M_1(0,t) = M_2(L,t), \tag{3.3}$$

$$\frac{dM_1}{dx_1}\Big|_{x_1=\ell} = \frac{G}{2}\frac{d\dot{u}_1}{dt} .$$

v^* may be found as suggested by Martin and Symonds [3] by minimizing $\Delta_o(v^*)$ where

$$\Delta_o(v^*) = \frac{1}{2}\int_S m(\dot{u}_i^o - v^*\phi_i(x_i))^2 ds + \frac{1}{2}\frac{G}{2}(V_o - v^*)^2,$$

i.e.

$$v^* = \frac{G/2\ V_o}{\int_S m\phi_i^2\ ds + \frac{G}{2}} \tag{3.4}$$

The equation of motion is from (2.13)

$$\frac{d^2M_i}{dx_i^2} + m\frac{d\dot{u}_i}{dt} = 0 \tag{3.5}$$

Substituting equations (3.1) and (3.2) in (3.5):

$$\frac{M_o v^{*\frac{1}{n}}}{\dot{\kappa}_o^{1/n}}\ T^{\frac{1}{n}}\ \frac{d^2}{dx^2}\ \phi_{ixx}^{\frac{1}{n}} = -mv^*\phi_i\dot{T}.$$

This equation is separable and gives

$$-\dot{T}\,T^{\frac{1}{n}} = \frac{M_o v^{*\frac{1}{n}}}{\dot{\kappa}_o^{1/n}\ mv^*\phi_i}\ \frac{d^2}{dx^2}\ \phi_{ixx}^{\frac{1}{n}} = A, \tag{3.6}$$

where A is a constant.

T(t) may then be found by integration. Taking into account the conditions $T(0) = 1$ and $T(t_f) = 0$ we get

$$T = \left(1 - \frac{t}{t_f} \right)^{\frac{n}{n-1}} , \tag{3.7}$$

where $t_f = \frac{n}{A(n-1)}$.

The shape functions $\phi_i(x_i)$ are governed by the differential equation

$$\frac{d^2}{dx_i^2} \phi_{ixx}^{\frac{1}{n}} = m\Lambda\phi_i , \tag{3.8}$$

where $\Lambda = \dfrac{Av^* \kappa_o^{\frac{1}{n}}}{M_o v^{*\frac{1}{n}}}$

and must satisfy the boundary conditions

$$\phi_1(0) = \phi_2(0) = \phi_{1x}(\ell) = \phi_{2x}(0) = 0 ,$$

$$\phi_{1xx}(0) = \phi_{2xx}(L) , \tag{3.9}$$

$$\frac{d}{dx} \phi_{1xx}^{\frac{1}{n}} \Big|_{x_1=\ell} = -\frac{G}{2} \Lambda ,$$

obtained by substituting (3.1) and (3.2) into (3.3).

Using the equations for rate of energy dissipation, it can be shown that

$$\Lambda = \frac{\int_S \phi_{ixx}^{\frac{n+1}{n}} \, ds}{\int_S m\phi_i^2 \, ds + \frac{G}{2}} . \qquad (3.10)$$

The iterative procedure adopted by Lee and Martin [5] and by Symonds [7] may be used to determine the shape functions $\phi_i(x_i)$ and hence the mode solution:

(i) Functions $\phi_i^{(0)}(x_i)$ which satisfy equations (3.9) and the normalizing condition $\phi_1(\ell) = 1$ are chosen;

$$\phi_1^{(0)}(x_1) = -\frac{x_1^2}{\ell^2} + \frac{2x_1}{\ell} ,$$

$$\phi_2^{(0)}(x_2) = -\frac{x_2^3}{2\ell^2 L} + \frac{x_2^2}{2\ell^2} .$$

(ii) Λ is determined using (3.10)

(iii) Writing $m\Lambda\phi_i(x)$ as the right-hand side of (3.8), the resulting equation is numerically integrated to give $\phi_i^{(1)}(x_i)$. This procedure is described in detail in Appendix A.

(iv) The generated function $\phi^{(1)}$ is normalized so that $\phi_1^{(1)}(\ell) = 1$ and is now used to calculate Λ and $m\Lambda\phi_i$. The cycle is repeated till Λ remains constant.

(v) v^*, t_f are calculated and the mode shape is thus fully determined.

The convergence of this procedure was not investigated but was found to be rapid.

3.2 Large deflection analysis

For the large deflection analysis, the total response is split into several intermediate stages to each of which the small deflection analysis is applied. The configuration at the end of each stage is used as the initial configuration of the next stage.

The mode solution is written as

$$\dot{u}_i = v^* \phi_i^{(t)}(x_i)\, T(t), \qquad (3.11)$$

where $\phi_i^{(t)}(x_i)$ is the instantaneous mode at the current deflections.

The initial configuration of the frame is shown in Figure 3.2.

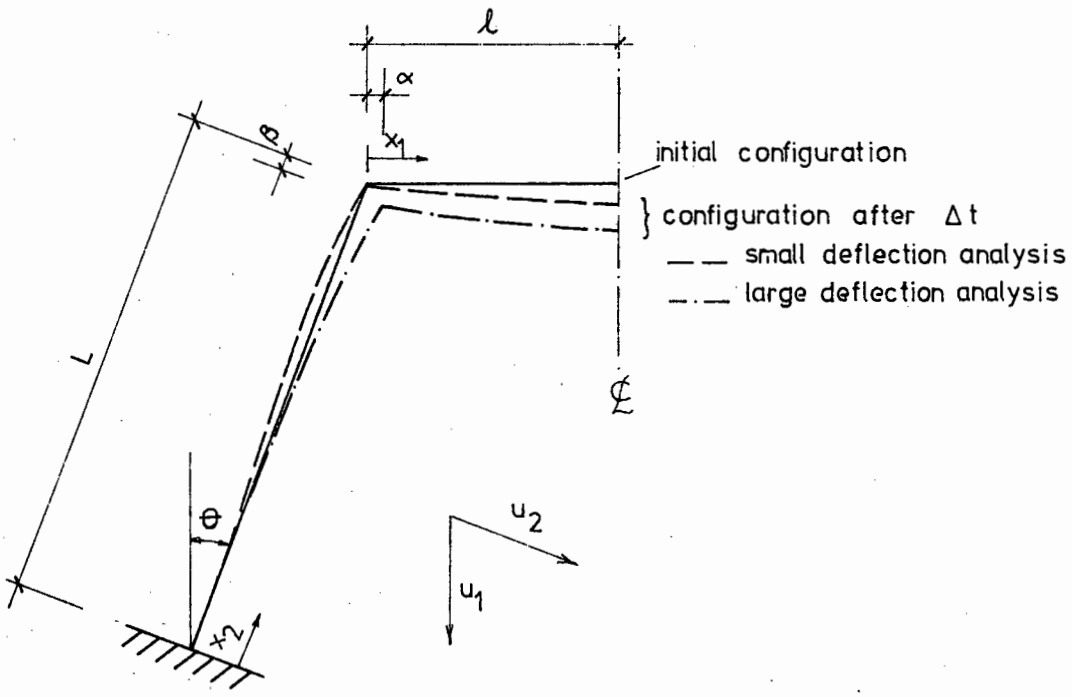

Figure 3.2

The initial mode shape is determined and assumed to govern the motion for a small period of time Δt after which the displacement shape of the frame is as shown in Figure 3.2. The small deflection analysis ignores geometry changes and assumes the corner point displacements to be zero. This is however not correct: the deflection of the beam member causes an inward displacement of the corner point

$$\alpha \approx \int_0^{\ell} \frac{1}{2}(u_{1x})^2 ds. \qquad (3.12)$$

The column displacement is then corrected using equation (3.13):

$$\bar{u}_2(x_2) = u_2(x_2) + \frac{4\alpha}{L^3}\left(\frac{x_2^4}{12L} + \frac{x_2^3}{6}\right)\frac{1}{\cos\theta} \tag{3.13}$$

The second term of equation (3.13) is an arbitrarily chosen interpolation function.

The axial shortening β due to the column deflection is then given by

$$\beta \approx \int_0^L \frac{1}{2}(u_{2x})^2 dx \tag{3.14}$$

The beam displacement must thus be corrected:

$$\bar{u}_1(x_1) = u_1(x_1) + \beta \cos\theta \tag{3.15}$$

The new configuration is thus determined and a new mode shape is calculated. The process is repeated till the frame comes to rest.

It must be noted that equation (3.13) only applies to the first time interval Δt. In the next stages, $u_2(L) \neq 0$ and $u_2(x_2)$ is simply sultiplied by the correction factor

$$\frac{\alpha}{u_2(L)}\ \frac{1}{\cos\theta} \tag{3.16}$$

to satisfy the continuity requirements.

For the rectangular frames, $\theta = 0$ and $\cos\theta$ is thus 1. The analysis remains otherwise the same.

4. Pulse loaded portal frames

Consider the portal frame described in the previous section. The frame is stationary at time t = 0 and the mass G (treated as a particle) is subjected to a load P given by

$$\begin{aligned} P &= P(t) \qquad \text{for} \qquad 0 \leq t \leq t_o, \\ P &= 0 \qquad\quad \text{for} \qquad\quad t > t_o. \end{aligned} \tag{4.1}$$

A mode form solution is sought:

$$\dot{u}_i(x_i,t) = v^* \phi_i^{(t)}(x_i)\, T(t), \quad i = 1,2 \tag{4.2}$$

where the mode function $\phi_1^{(t)}(x_1)$ is defined so that $\phi_1(\ell) = 1$, and the time function T(t) so that $T(0) = 0$, $T(t_o) = 1$ and $T(t_f) = 0$.

The boundary conditions to be satisfied are the same as those given in (3.3) for $t > t_o$. However, for $t < t_o$

$$\left.\frac{dM_1}{dx_1}\right|_{x_1=\ell} = \frac{G}{2}\frac{d\dot{u}_1}{dt} - \frac{P}{2}. \tag{4.3}$$

The equation of motion is again

$$\frac{d^2M_i}{dx_i^2} + m\frac{d\dot{u}_i}{dt} = 0 \tag{4.4}$$

For $t > t_o$, the solution procedure will thus be the same as for the impulse case, large deflection analysis. For $t \leq t_o$,

equation (3.6) is still valid i.e. the differential equation governing the shape function $\phi_i^{(t)}(x_i)$ is

$$\frac{d^2}{dx^2}\,\phi_{ixx}^{\frac{1}{n}} = -\phi_i\,\frac{mv^*\dot{\kappa}_o^{\frac{1}{n}}\,\dot{T}}{M_o v^{*1/n} T^{1/n}} \tag{4.5}$$

and the equation governing the time function T(t) is

$$-\dot{T}\,T^{\frac{1}{n}} = A. \tag{4.6}$$

Integrating (4.6) and taking into account the conditions $T(0) = 0$, $T(t_o) = 1$:

$$T = \left(\frac{t}{t_o}\right)^{\frac{n}{n-1}} \tag{4.7}$$

Equation (4.5) becomes then

$$\frac{d^2}{dx^2}\,\phi_{ixx}^{\frac{1}{n}} = \phi_i\,\frac{mv^*\dot{\kappa}_o^{\frac{1}{n}}\,n}{M_o v^{*1/n}\,t_o(1-n)} \tag{4.8}$$

Substituting (3.1), (4.2) and (4.7) in (4.3), the boundary condition at $x_1 = \ell$ becomes

$$\frac{d}{dx_1}\,\phi_{1xx}^{\frac{1}{n}}\Big|_{x_1=\ell} = \frac{Gv^*\dot{\kappa}_o^{\frac{1}{n}}\,n}{2M_o v^{*1/n}\,t_o(1-n)} - \frac{P\dot{\kappa}_o^{\frac{1}{n}}}{2M_o v^{*1/n}}\left(\frac{t_o}{t}\right)^{\frac{1}{n-1}} \tag{4.9}$$

In pulse loaded structures where the initial velocities are zero, v^* cannot be determined by minimizing $\Delta_o(v^*)$.

Using the work rate equation

$$\int_S \frac{P}{2}\dot{u}_i ds - \int_S m\ddot{u}_i\dot{u}_i ds = \int_S M_i\dot{\kappa}_i ds , \qquad (4.1))$$

integrating both sides over the time interval $[0,t_o]$ and introducing (3.1), (4.2) and (4.7) we get

$$\frac{I}{2} - v^*\left[\int_S m\phi_i^2 ds + \frac{G}{2}\right] = \frac{M_o v^{*\frac{1}{n}} t_o^{(n-1)}}{\dot{\kappa}_o^{1/n}\, n}\int_S \phi_{ixx}^{\frac{n+1}{n}} ds , \qquad (4.11)$$

where $I = \int_o^{t_o} P dt$ = impulse.

If $\phi_i(x_i)$ is known, v^* may be determined by (4.11). It is clear from (4.9) that mode solutions do not exist. It will however be assumed here that $\phi_i(x_i)$ may be approximated by the initial mode shape of the impulse loading case. The following procedure may then be used for the analysis:

(i) The initial mode shape is determined as in the impulse loading case. This is used to calculate v^*. The configuration of the frame at time t_o is given by

$$\dot{u}_i = v^*\,\phi_i(x_i)\left(\frac{t}{t_o}\right)^{\frac{n}{n-1}} . \qquad (4.12)$$

(ii) This is then used as the initial configuration for the next phases which are treated as in the large deflection impulse loading case.

A series of frames was studied using the methods described here; the results are given in Part II, section 3.

PART II: EXPERIMENTAL STUDY

Two series of experiments were conducted to test the validity of the mode form solution applied to portal frames: the first on rectangular frames, the second on trapezoidal frames.

1. The Specimens

1.1 Specimen material

The frames were made from commercial mild steel (carbon content < 0,15 %). The finished test specimens were heat-treated in a barium salt bath for 1 hour at 700° C. Tensile specimens - as specified in ASTM E8 [24] - were tested at four speeds up to a maximum of 0,05 sec^{-1} strain rate. Tables 1 and 2 show the results of these tests: the σ_o values were obtained by putting the measured dynamic yield stress into the formula

$$\frac{\sigma_y}{\sigma_o} = \left(1 + \left(\frac{\dot{\varepsilon}}{40}\right)^{\frac{1}{5}}\right) .$$

All theoretical calculations were done with the average σ_o at the highest strain rate (0,05 sec^{-1}). For the rectangular frames, σ_o = 238,350 MPa. For the trapezoidal frames, σ_o = 216,533 MPa. Other material properties are:

ρ = mass density = 7 724,359 kg/m^3 for the rectangular frames

= 7 888,889 kg/m^3 for the trapezoidal frames

E = Young's modulus = 200 GPa

Specimen Number	$\dot{\varepsilon}$ (sec^{-1})	σ_y (MPa)	σ_o (MPa)	Average σ_o
8	$4{,}704.10^{-5}$	233,502	219,215	
13		238,298	223,717	
16		239,340	224,695	224,725 ±
2		246,345	231,272	4,975
15	$4{,}704.10^{-4}$	246,637	223,546	
1		261,245	236,786	
18		251,831	228,253	231,476 ±
14		261,833	237,319	6,723
3	$4{,}704.10^{-3}$	277,284	238,275	
21		279,485	240,167	
10		281,544	241,936	239,633 ±
5		277,284	238,275	1,758
20	$4{,}704.10^{-2}$	296,256	235,223	
9		305,013	242,176	
11		309,391	245,652	
4		299,175	237,541	
12		297,137	235,923	238,350 ±
6		294,195	233,587	4,625

Overall average: σ_o = 234,087 ± 7,426 MPa

TABLE 1

Tensile tests for rectangular portal frames

Specimen Number	$\dot{\varepsilon}$ (sec^{-})	σ_y (MPa)	σ_o (MPa)	Average σ_o
7	$4,98.10^{-5}$	187,432	175,840	
2		183,143	171,816	
5*		274,714	257,724	175,177 ±
1		189,602	177,876	3,084
8	$4,98.10^{-4}$	221,200	200,275	196,752 ±
12		213,417	193,228	4,983
9	$4,98.10^{-3}$	237,514	203,771	204,996 ±
3		240,370	206,221	1,732
4	$4,98.10^{-2}$	273,606	216,727	
11		276,497	219,017	
10		270,424	214,206	216,533 ±
6		272,917	216,181	1,979

Overall average: 199,560 ± 17,519 MPa

TABLE 2

Tensile tests for trapezoidal frames

* Disregarded

1.2 The Frames

The frames were made from mild steel strips. These were surface ground on four faces and then bent to the required dimensions. Three types of frames were tested: typical dimensions are given in Figures 1 and 2. Steel blocks (weighing less than 3 g) were silver braised at the corners to ensure that plastic hinges did not form at the corners where the cross-section is not uniform. These blocks have been neglected in the theoretical calculations.

The frames were then heat-treated as described earlier. A total of 30 specimens were designed, 18 of which were rectangular frames and 12 of which were trapezoidal frames. Of the rectangular frames, 9 had a height of 129 mm, and 9 had a height of 180 mm, the span remaining constant. These will be referred to as the small and large rectangular frames respectively. Steel blocks were bolted to the beam members at mid span. The blocks attached to the rectangular frames weighed 108,9 g; those attached to the trapezoidal frames weighed 104,3 g.

2. Experimental Details

The loads were applied by fitting commercial electric detonators enclosed in steel containing cylinders. The cylinders were fixed to the centre mass with plasticine so that they disengaged from the attached mass at the instant of firing i.e. they did not contribute to the attached mass. Different loading conditions were obtained by varying the dimensions of

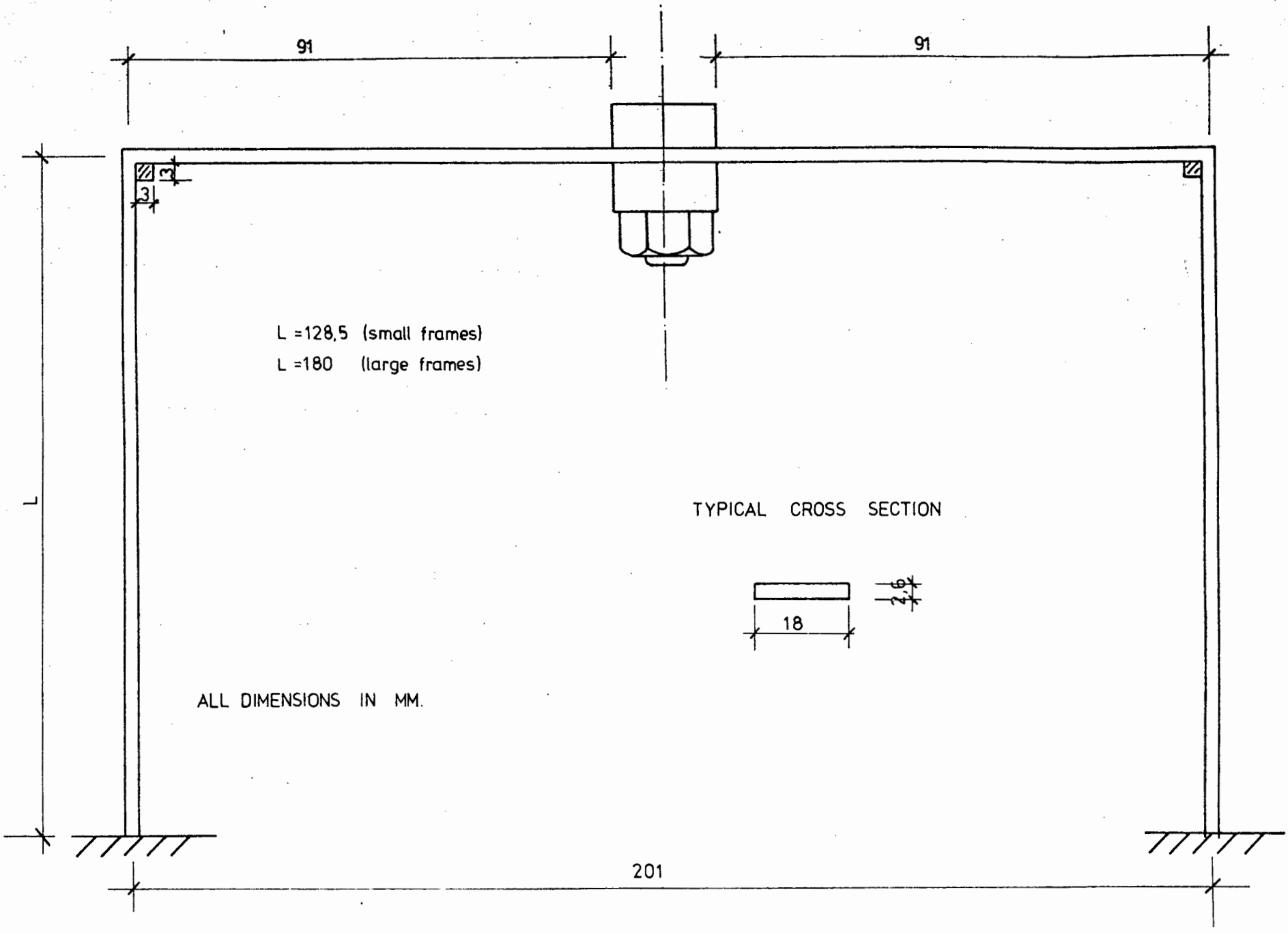
91
91
3
3
L =128,5 (small frames)
L =180 (large frames)
L
TYPICAL CROSS SECTION
2,6
18
ALL DIMENSIONS IN MM.
201

FIG. 1

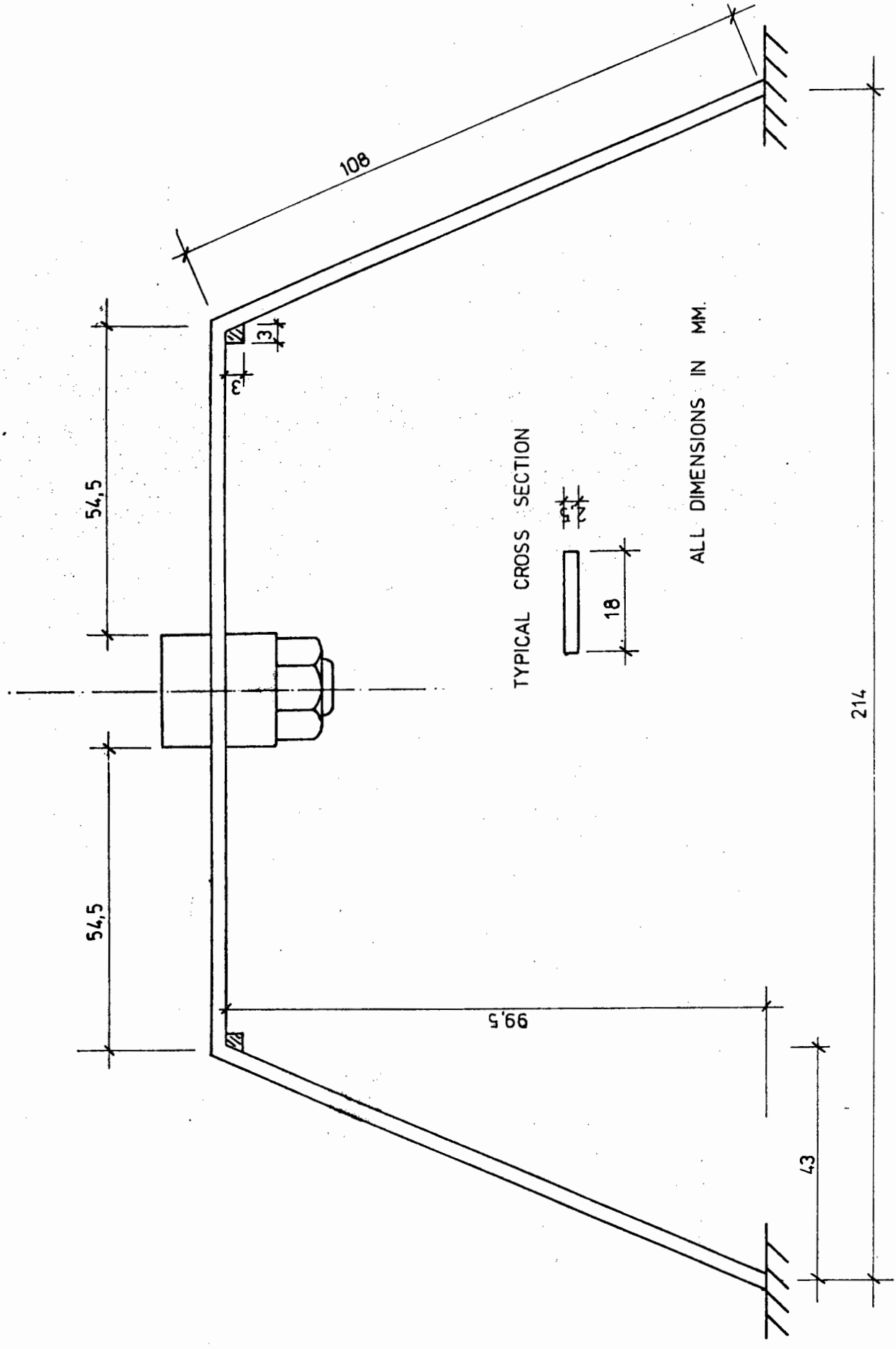
108
54,5
54,5
99,5
214
43
3
3
TYPICAL CROSS SECTION
18
ALL DIMENSIONS IN MM.

FIG. 2

the containing cylinders and the number of detonators. The loading time was very short (less than 0,6 msec) and the load could thus be treated as an impulse.

The requirements of the testing apparatus were to provide a means of measuring

i) the impulse produced by the detonators, and

ii) the transient velocity time response of the centre mass.

This was achieved by attaching the frame specimens to a ballistic pendulum and fixing a velocity transducer onto the centre mass. Figure 3 illustrates the experimental arrangement employed.

2.1 The ballistic pendulum

The ballistic pendulum was used to measure the impulse applied by the detonator. The impulse is directly related to the amplitude of oscillation of the pendulum through the conservation of momentum equation. This experimental technique has been used in several laboratories [19, 20, 21] with apparent success. Two important assumptions underlie the method:

i) gas pressures from the explosion only act on the centre mass i.e. no external impulses are applied to the pendulum other than those exerted by the specimen through its support reactions and

ii) the amplitude of oscillation of the pendulum is not affected by the finite duration of the impulse.

'Blast shields' have been used in certain laboratories [20, 21] to shield the pendulum from unwanted pressures. It was felt here that these would not be necessary since the detonators were enclosed in steel cylinders so that the blast pressures were confined to the attached mass only.

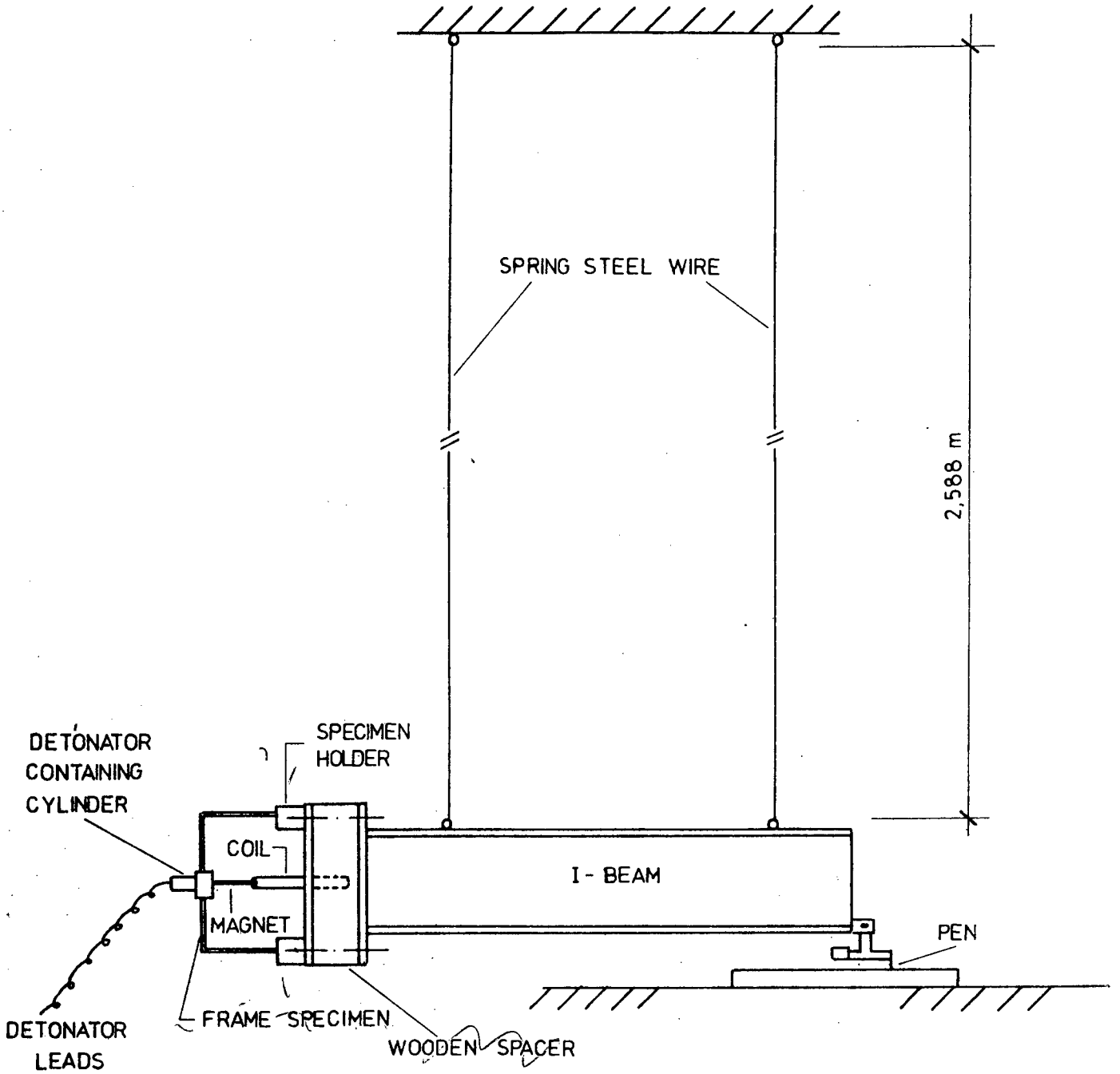
SPRING STEEL WIRE
2,588 m
DETONATOR CONTAINING CYLINDER
SPECIMEN HOLDER
COIL
MAGNET
I - BEAM
PEN
DETONATOR LEADS
FRAME SPECIMEN
WOODEN SPACER

FIG. 3

The second assumption was validated on the basis of the following two degree of freedom model. The frame-pendulum system is idealised as shown in Figure 4.

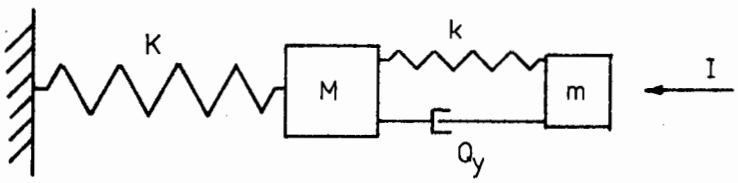

Figure 4

The pendulum of mass M is attached to a massless elastic spring of stiffness $K = 4\pi^2 M/T^2$. The attached mass m is connected to M through an elastic plastic spring of elastic slope k and yield stress Q_y where k and Q_y correspond to the elastic stiffness and collapse load of the frame respectively. The mass m is slightly modified to include the weight of the frame. An impulse $I = P.t_o$ is applied on m (P is a rectangular load pulse such that $P = P_o$ for $t < t_o$; $P = 0$ for $t > t_o$). This model was analysed keeping I constant but varying t_o from 0 to 1 msec. It was found that the amplitude of oscillation of the mass M varied by less than 0,3 mm for I = 3 Nsec (typical impulse used in the experiments).

2.1.1 Relation between the impulse I and the amplitude of oscillation of the pendulum Δ

The pendulum is shown diagrammatically in Figure 5.

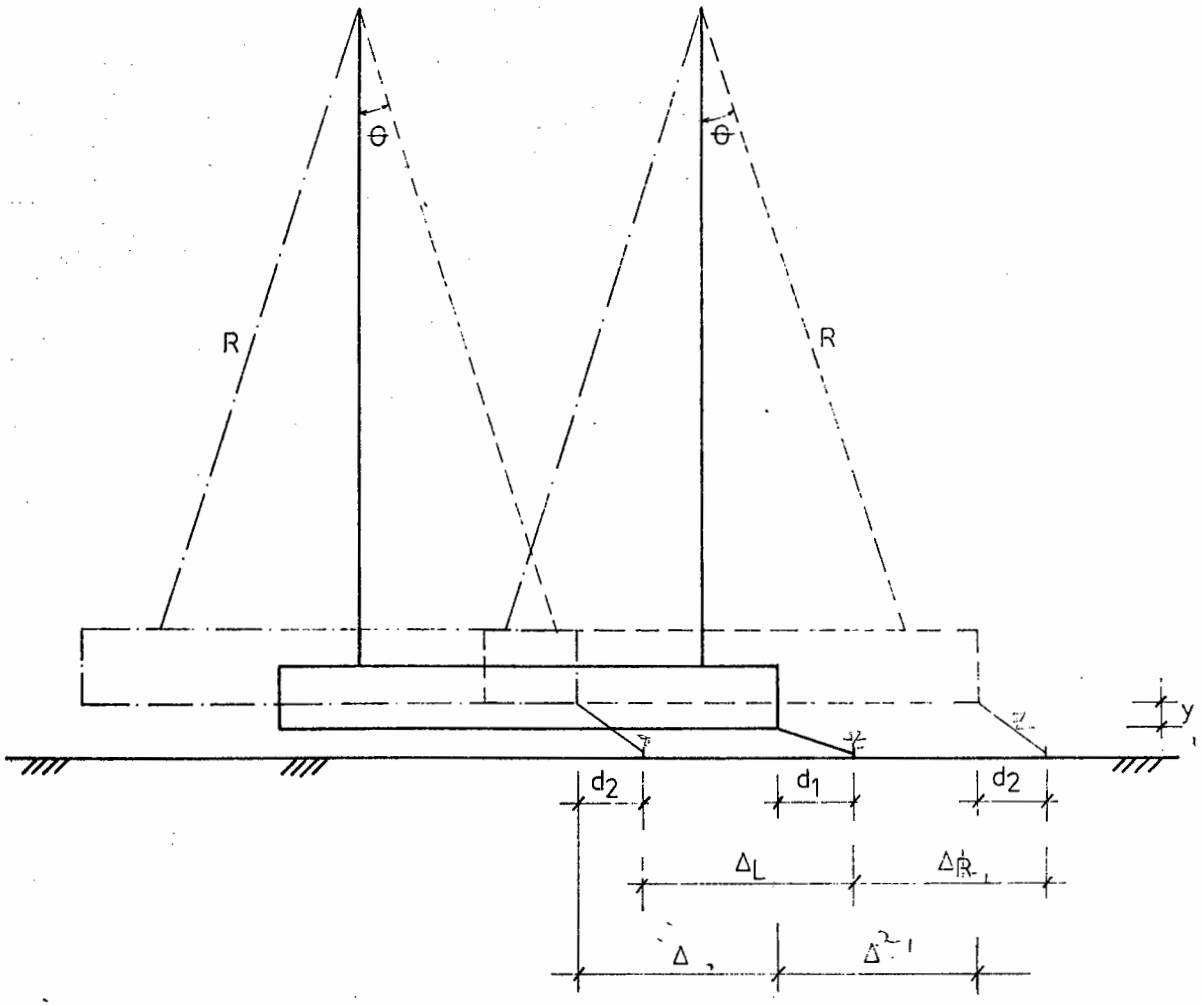

Figure 5

Let M be the mass of the pendulum and frame,

m the mass of the attached mass,

v_o the instantaneous velocity of the attached mass,

v the velocity of the pendulum after impulse.

If the impulse duration is neglected, the initial momentum of the system is that of the attached mass mv_o, and the momentum of the system just after the impulse is $(m + M)v$ so that

$$mv_o = (m + M)v. \tag{1}$$

The pendulum then swings to a maximum height y. Using the conservation of mechanical energy for this part of the motion:

$$\tfrac{1}{2}(m + M)v^2 = (m + M)gy. \tag{2}$$

From (1) and (2) we get

$$v_o = \frac{m + M}{m}\sqrt{2gy}. \tag{3}$$

It is now necessary to relate y to the horizontal displacement of the pendulum Δ:

$$\Delta \approx R\theta,$$

$$y \approx \frac{R\theta^2}{2} = \frac{\Delta^2}{2R}. \tag{4}$$

(3) and (4) give

$$v_o = \frac{\Delta}{R} \frac{(m + M)}{m} \sqrt{gR} \ . \qquad (5)$$

It can be seen in Figure 5 that the displacement of the pendulum to the right (Δ_R) and left (Δ_L) of the equilibrium position are not the same and are different to the horizontal displacement of the pendulum. However, since

$$\Delta_R = \Delta + d_2 - d_1$$

$$\text{and} \quad \Delta_L = \Delta - d_2 + d_1 \ , \qquad (6)$$

$$\text{we get} \quad \Delta = \frac{\Delta_L + \Delta_R}{2}$$

The impulse may then be determined:

$$I = mv_o$$

2.1.2 Evaluation of the friction in the system

All the above equations are valid provided the system is frictionless and stable. Stability was ensured by designing the apparatus so that the impulse would be applied at a point about the same level as the centre of gravity of the suspended mass. To reduce the friction of the pendulum, its weight was counter-balanced as shown in Figure 6.

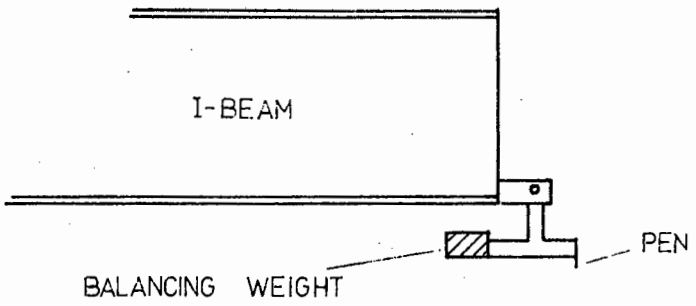

Figure 6

The amount of friction in the system was assessed in the following way. If a viscous damping force is assumed, the equation of motion of the pendulum is

$$M\frac{d^2x}{dt^2} + c\frac{dx}{dt} + \frac{M}{R}gx = 0, \qquad (7)$$

where c is the damping coefficient.

Letting $\beta = \frac{c}{2M}$ and $\omega = \sqrt{\frac{g}{R}}$, (7) becomes

$$\frac{d^2x}{dt^2} + 2\beta\frac{dx}{dt} + \omega^2 x = 0. \qquad (8)$$

The solution of this equation is given by

$$x = e^{-\beta t}\frac{\dot{x}_o}{\omega_d}\sin\omega_d t\ , \qquad (9)$$

where $\omega_d^2 = \omega^2 - \beta^2$.

The displacement is maximum when

$$\dot{x} = x(\omega_d \cot \omega_d t - \beta) = 0,$$

$$\text{i.e.} \quad x_{max} = e^{-\frac{\beta\alpha}{\omega_d}} \frac{\dot{x}_o}{\omega_d} \sin \alpha, \tag{10}$$

$$\text{where} \quad \alpha = \arctan \frac{\omega_d}{\beta}.$$

The initial velocity of the pendulum is then

$$v_o = x_{max} \frac{e^{\frac{\beta\alpha}{\omega_d}}}{\sin \alpha} \omega_d. \tag{11}$$

If the system was frictionless, we would have

$$v_o^* = x_{max} \omega, \tag{12}$$

$$\text{i.e.} \quad \frac{v_o^*}{v_o} = \frac{\sin\alpha}{e^{\frac{\beta\alpha}{\omega_d}}} \cdot \frac{\omega}{\omega_d}. \tag{13}$$

To determine β, the pendulum was allowed to swing freely over a number of cycles with different initial amplitudes. It was observed that the loss in amplitude of the swing per quarter cycle was less than 0,5 % i.e.

$$c \approx \frac{\ell n\, \delta}{\pi} M \sqrt{\frac{g}{R}} = 0{,}085 \quad ,$$

where δ is the logarithmic decrement.

This gives $\frac{\dot{v}_o^*}{v_o} = 0{,}999$ and the friction was thus ignored herein.

2.2 The velocity transducer

In some preliminary tests, a piezo-electric accelerometer was attached to the centre mass to record the acceleration during the test. The presence of high frequency elastic vibrations made the record very difficult to interpret, and the accelerometer was discarded in favour of a velocity transducer (Rawlings [9] has reported the same problem with an accelerometer). The transducer is shown diagrammatically in Figure 7.

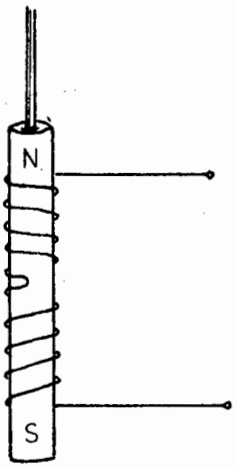

Figure 7

A permanent magnet core moves inside a form wound with two coils and generates a voltage

$$E = Blv,$$

where B is the flux density,

l is the length of the coil,

v is the relative velocity of coil and magnet.

To calibrate the transducer, a small motor with eccentric shaft was used to drive the magnet core. A sinusoidal velocity of known maximum amplitude was thus generated. The calibration curve is shown in Figure 8. The linear range was found to be limited to 20 mm. For deformations greater than 30 mm, the transducer was only used to record the pulse duration and the time to maximum deformation. The calibration was checked at the beginning of each series of experiments to make sure that the flux density had not been affected during the previous experiments.

All calibrations were however done at low velocities (0,283 m/s). No means could be found to calibrate the transducer at higher velocities (typically 15 to 20 m/s in experiments) and it was assumed that the same calibration curve applied at higher velocities.

Table 1 gives a comparison between maximum velocities from the transducer and the pendulum (in which case pulse duration is ignored).

Frame	Pendulum	Transducer
8R*	14,29 m/s	13,85 m/s
16R	14,94	14,62
9R	14,12	13,85
15R	15,09	14,62
11R	14,57	12,31
5T*	15,32	14,30
11T	15,45	15,40
9T	17,15	15,20
6T	17,57	15,50

*R : Rectangular frame T : Trapezoidal frame

TABLE 1

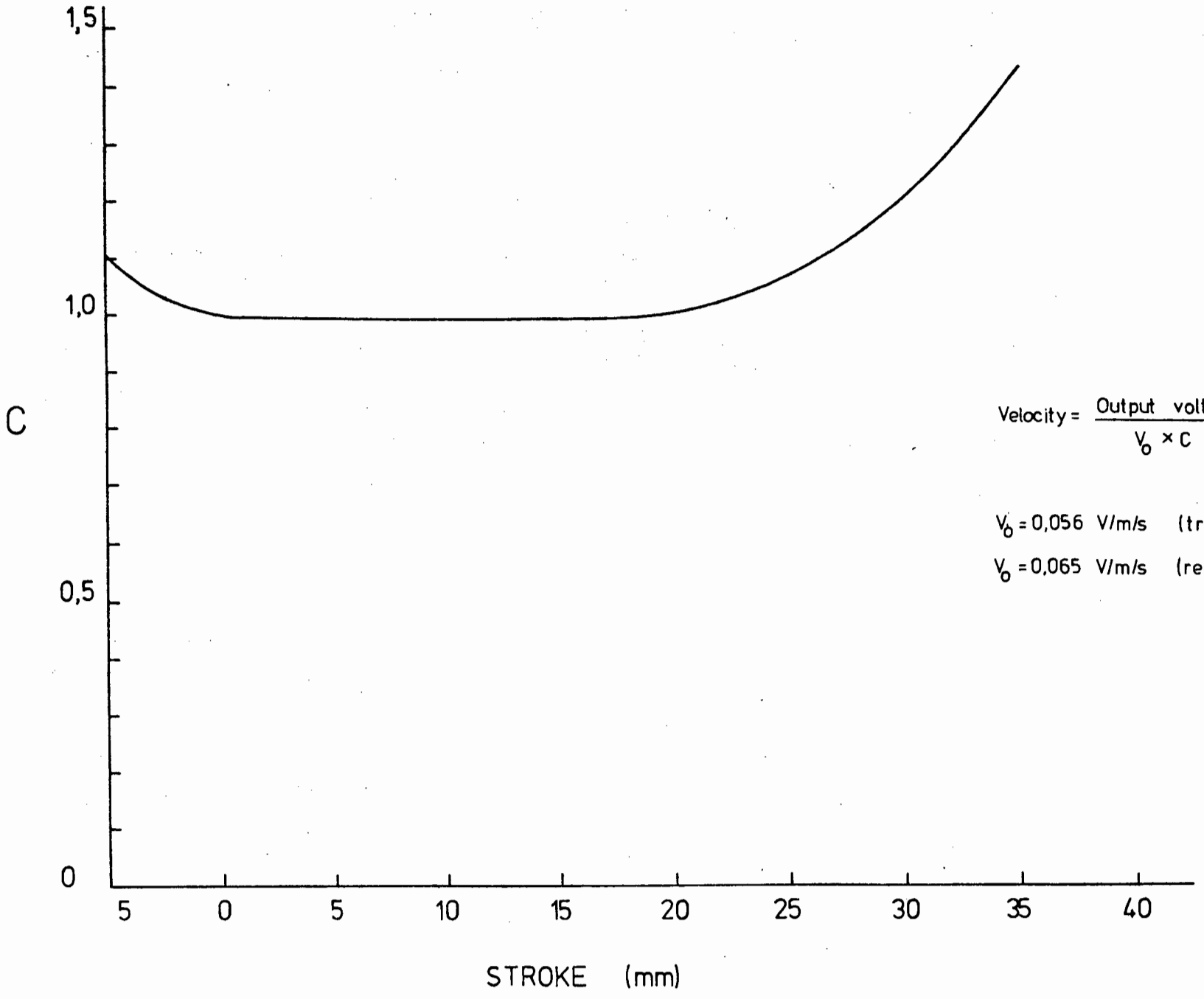

$$\text{Velocity} = \frac{\text{Output voltage}}{V_0 \times C}$$

$V_0 = 0{,}056$ V/m/s (trapezoïdal frames)

$V_0 = 0{,}065$ V/m/s (rectangular frames)

FIG. 8

Table 1 only compares velocities which are less than ± 17 m/s. It can be seen that the pendulum and transducer readings compare very well. However, for velocities greater than ± 17 m/s, the discrepancies become larger (up to 20% at ± 22 m/s). It must be noted that the transducer was then well into its non-linear range. The arrangement shown in Figure 8 was used to record the transducer output voltage.

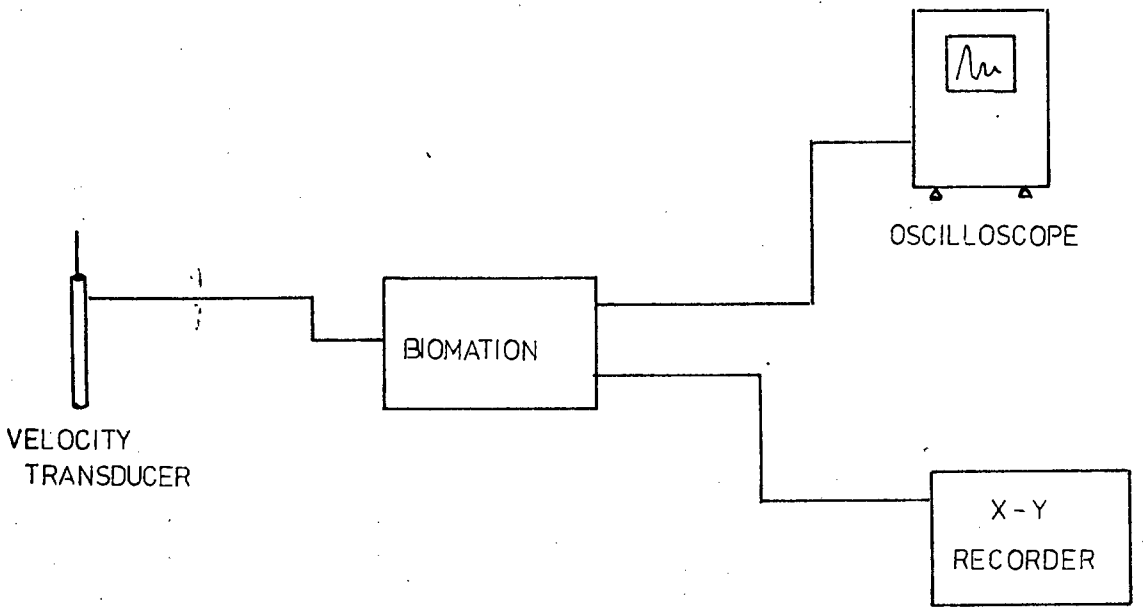

Figure 8

The output voltage is recorded in the biomation as a function of time. The amplitude versus time information is stored in it in digital form. A reconstructed analog signal is then provided by the biomation for viewing on the oscilloscope or making a permanent record on the chart recorder.

3. Results

The following figures and tables summarize the test results. These will be further discussed in the next section. All theoretical calculations were done using the techniques described in Part I.

In the following pages, experimental and theoretical results are compared. Figures 9, 10 and 11 show the deflection profiles of the frames. Figures 12, 13, 14 and 15 show the transient response of the attached mass. Figures 17 and 18 give the final deflection of the centre mass as a function of the applied impulse. Figures 19 and 20 give the final inward displacement at the corner point as a function of the applied impulse. Figures 20 and 21 compare the observed time to maximum deformation with computed deformation times. Tables 2, 3 and 4 give a full summary of the experimental and theoretical results.

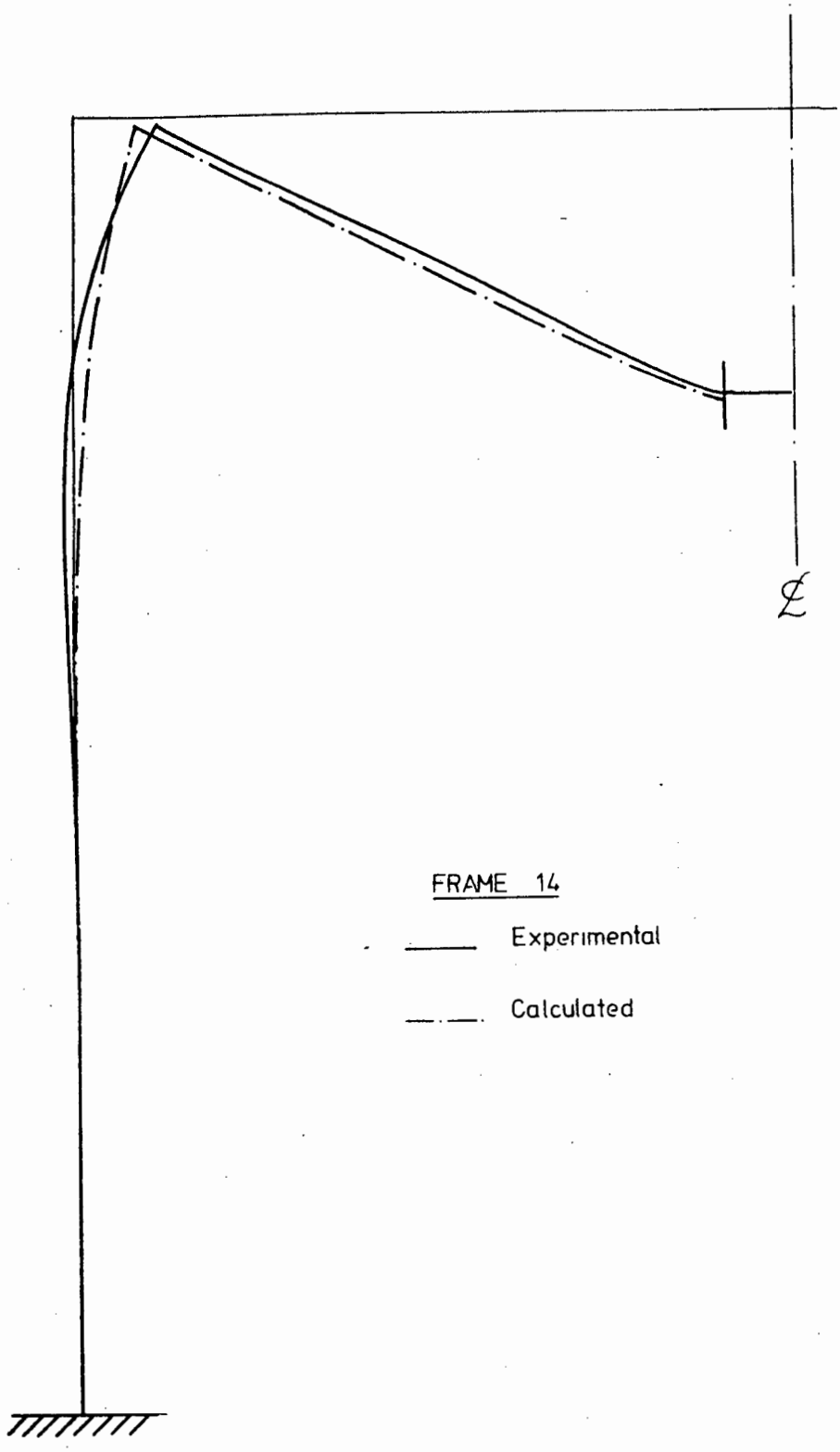

Figure 9 Full scale deflection profiles of a large rectangular frame as observed and as calculated (including pulse duration). The difference between observed and calculated curves are as would be expected since the assumptions in the theoretical calculations are all conservative (the calculations also omit the initial phase of the response).

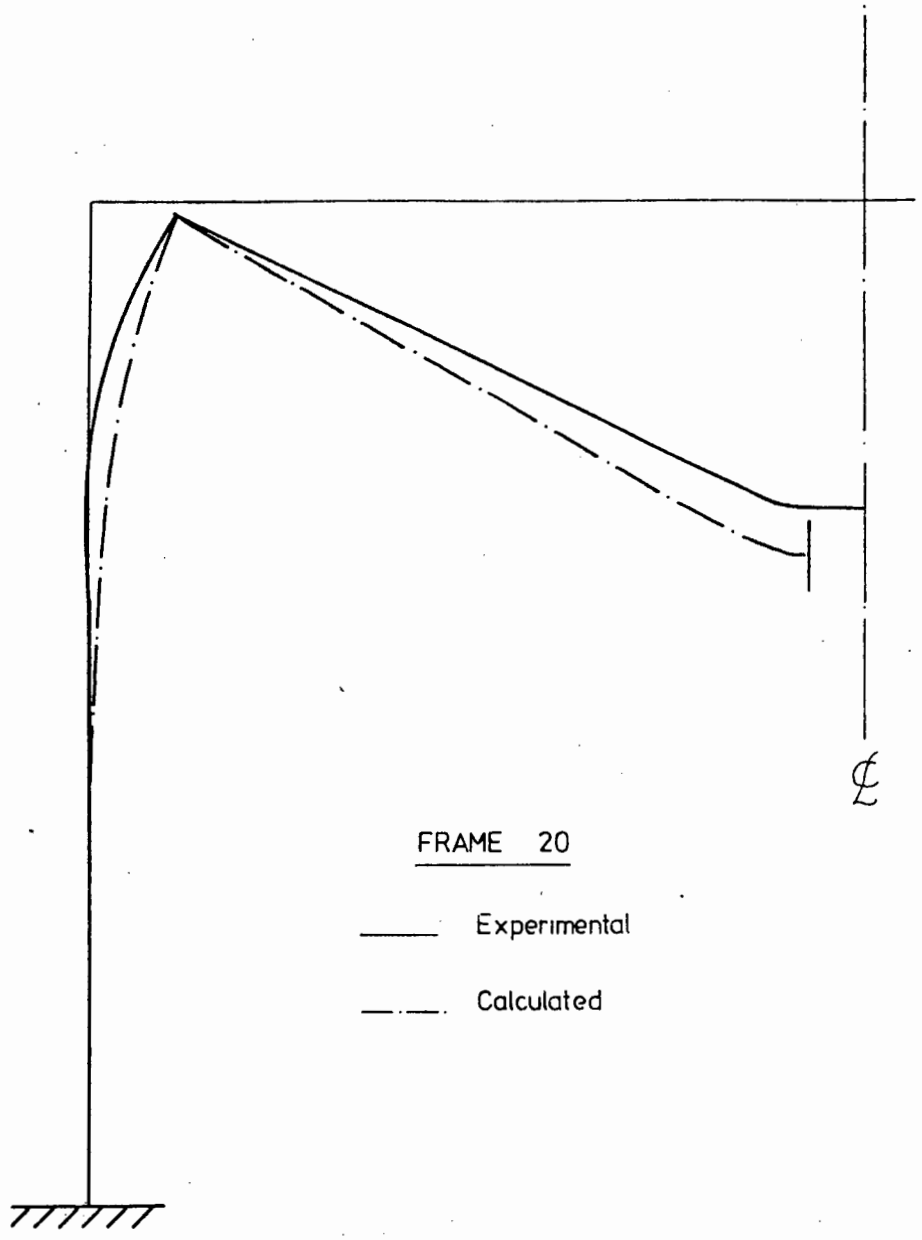

Figure 10 Full scale deflection profiles of a small rectangular frame as observed and as calculated (ignoring the pulse duration). The difference between theory and experiment is larger here since ignoring the pulse duration makes the calculations even more conservative.

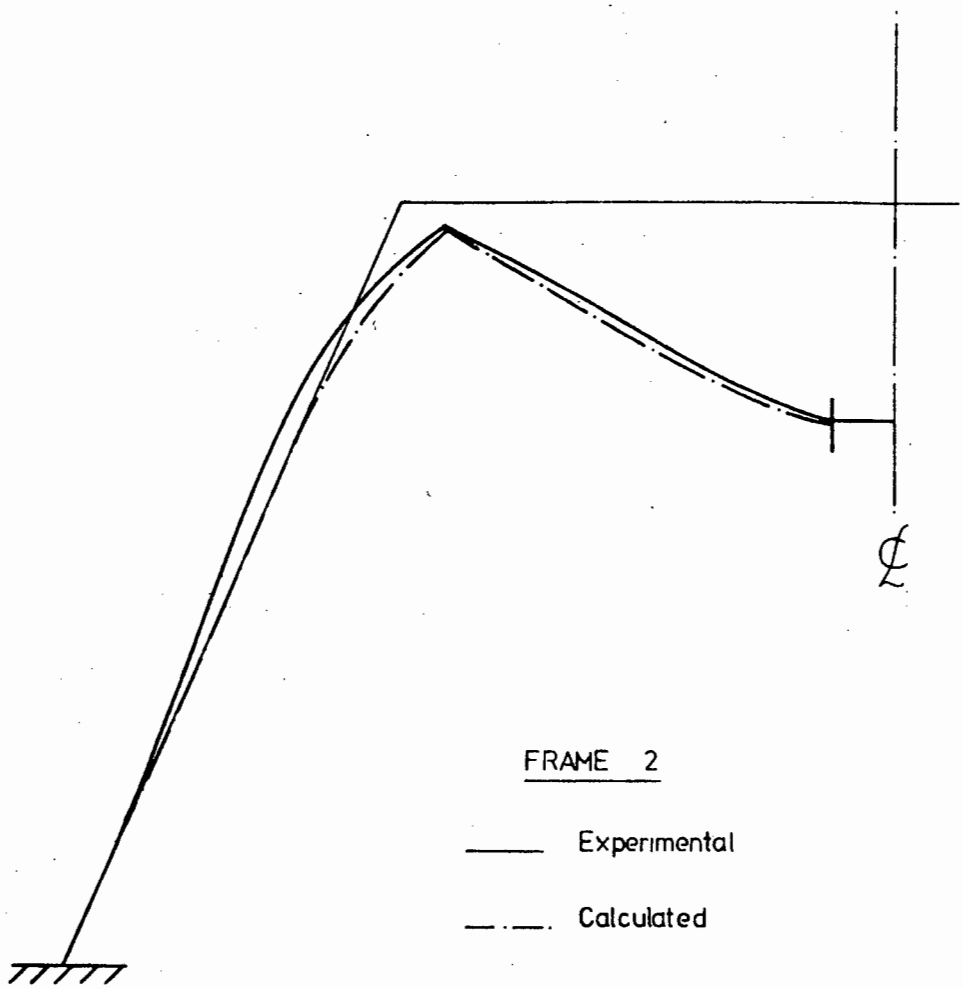

Figure 11 Full scale deflection profiles of a trapezoidal frame as observed and as calculated (including pulse duration).

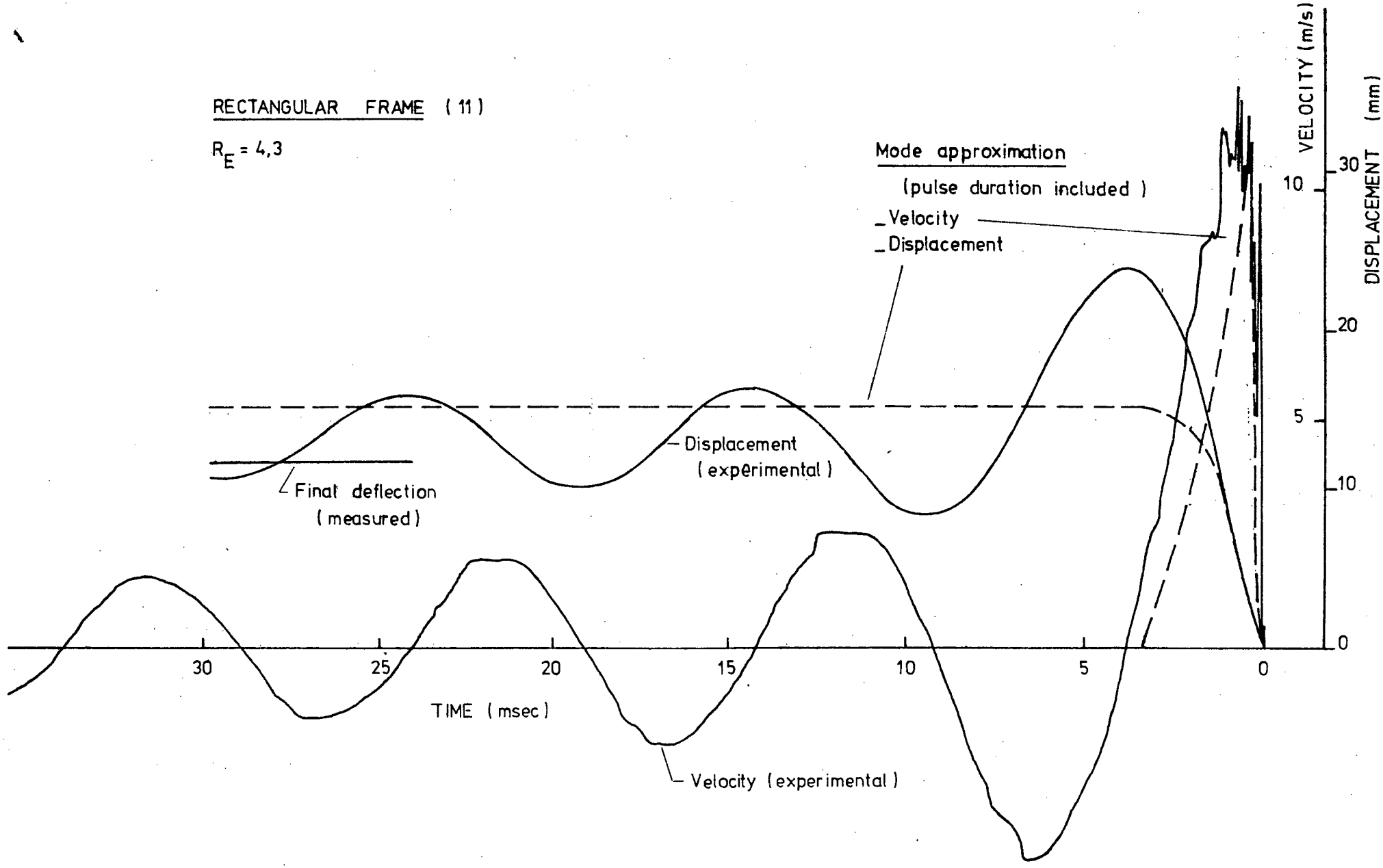

Figure 12 Transient response of the attached mass (mid-point) of beam member.
Note the high frequency response of the initial phase of the motion.
The experimental displacement curve was obtained by numerically integrating the velocity curve.

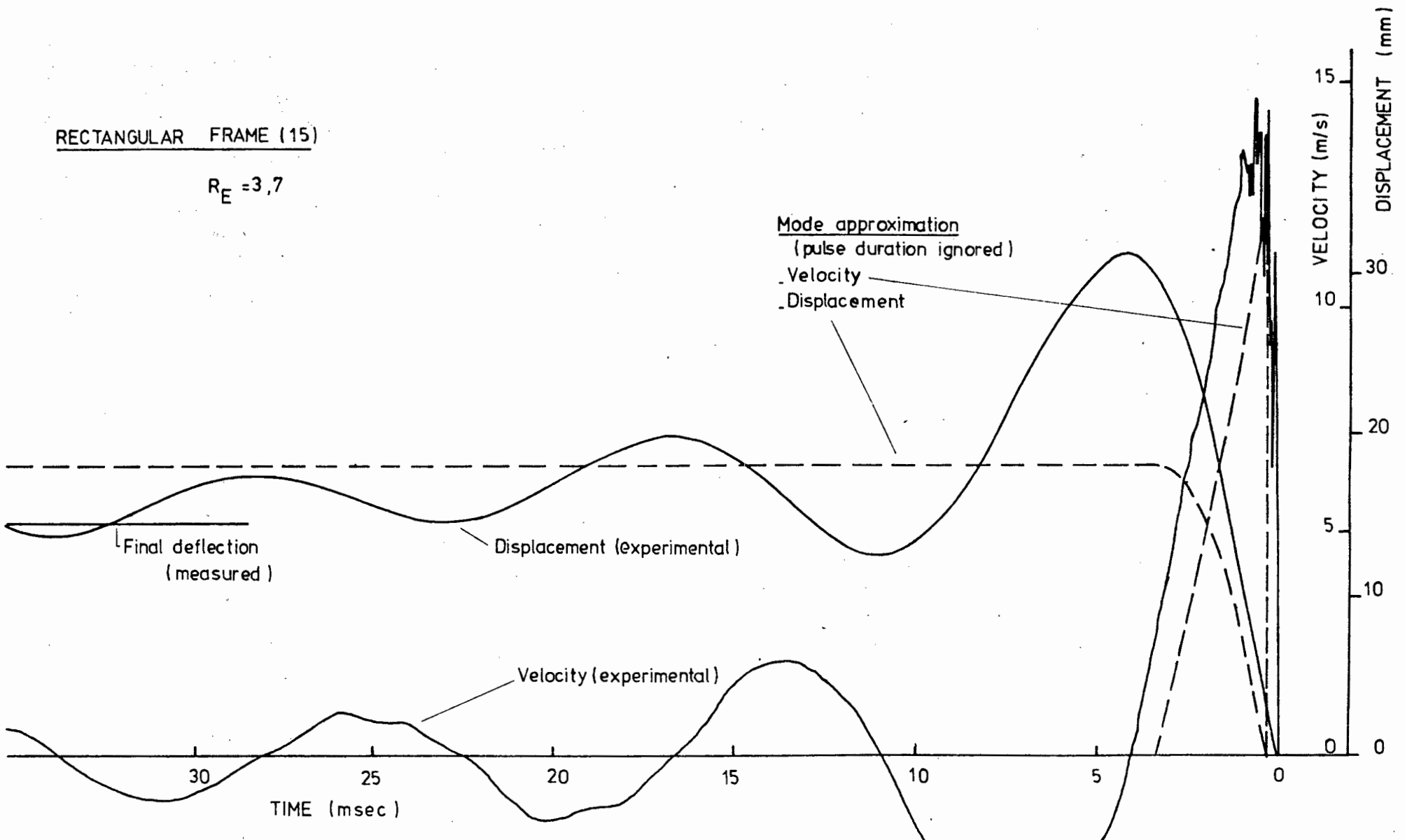

Figure 13 Transient response of the attached mass-small rectangular frame. The close agreement between the measured final displacement and the one obtained from the displacement curve shows that the velocity transducer calibration curve is valid at these velocities.

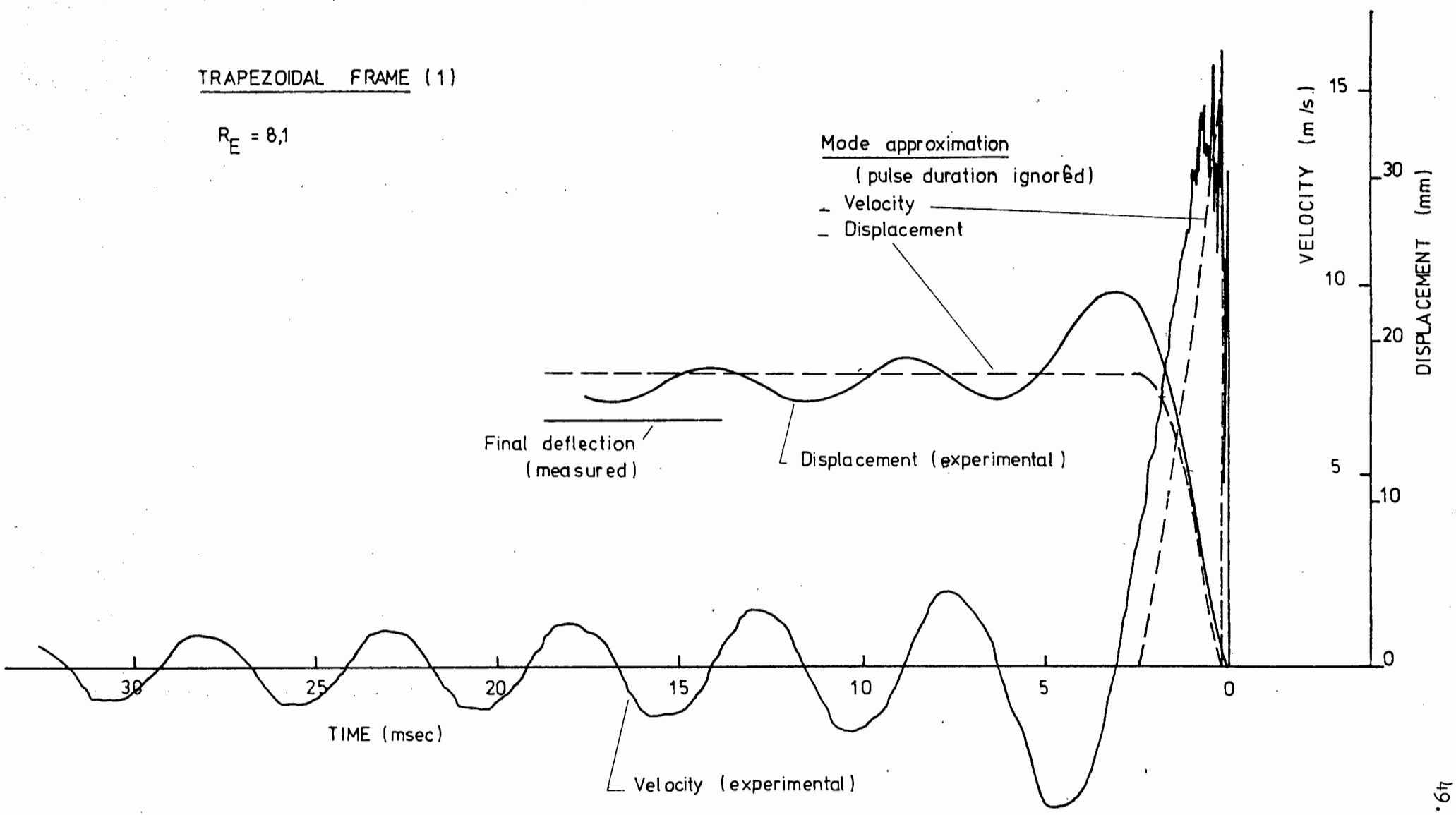

Figure 14 Transient response of the attached mass-trapezoidal frames.

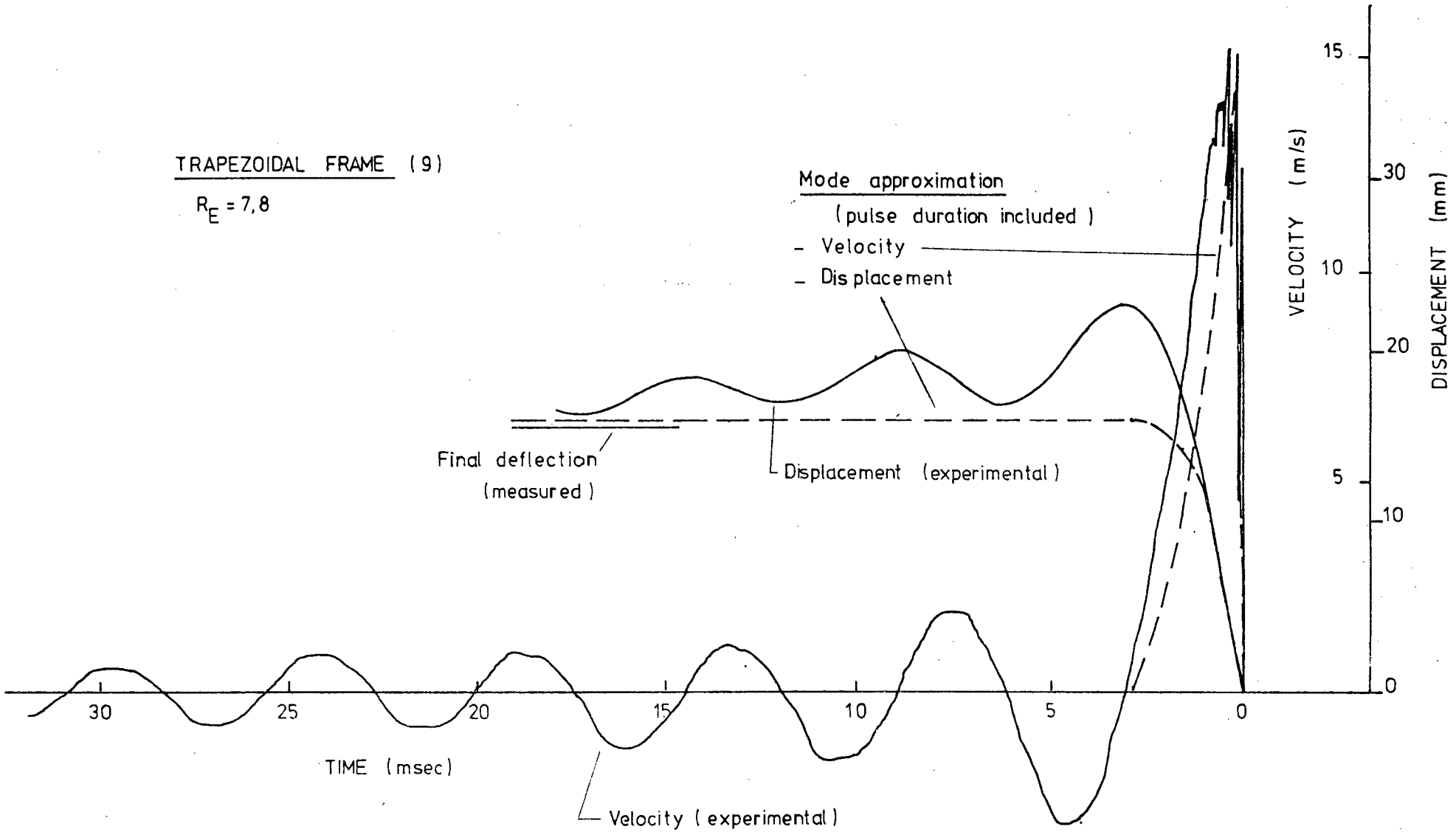

Figure 15 Transient response of the attached mass-trapezoidal frames.

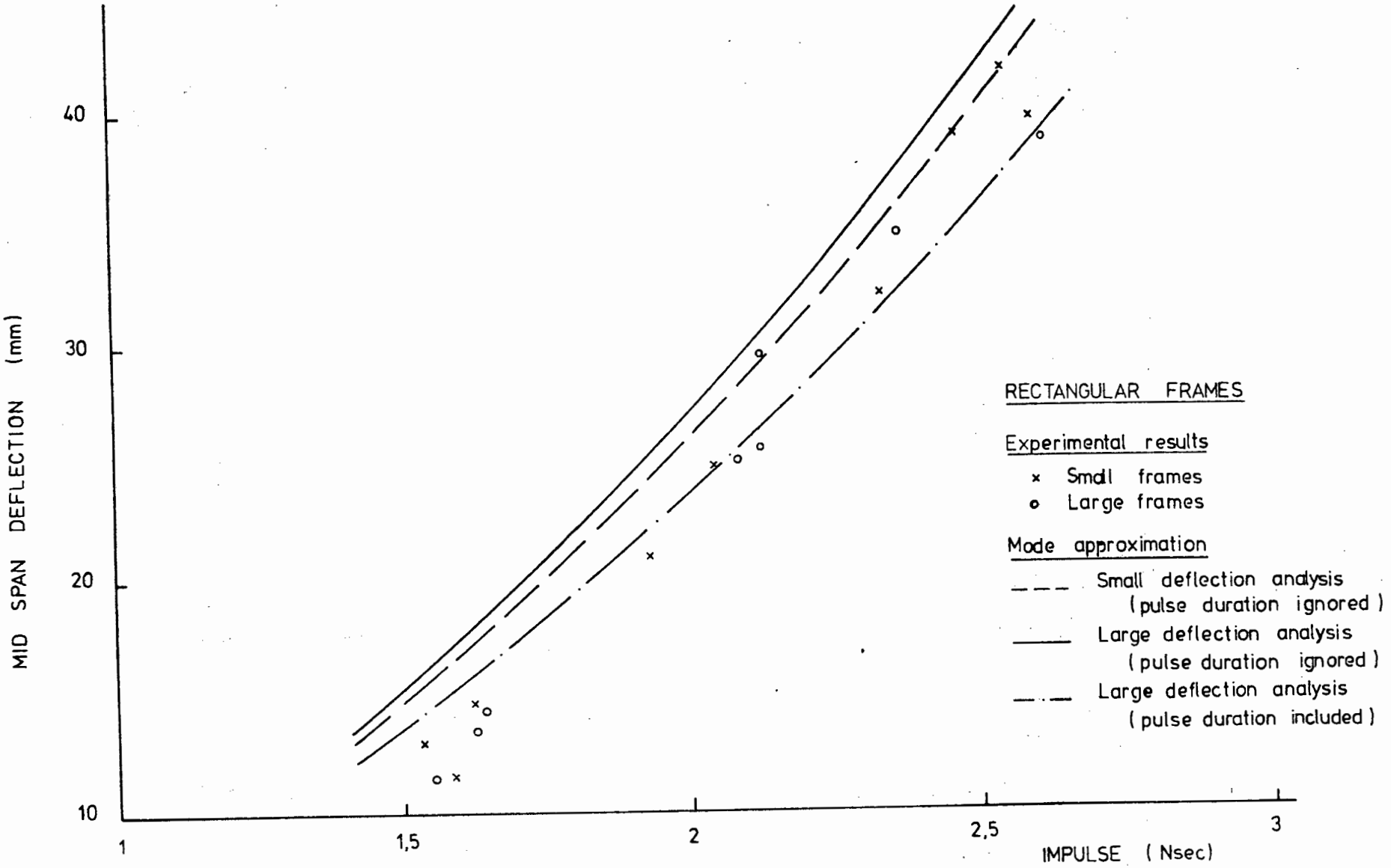

Figure 16 Summary of tests on the rectangular frames showing the final deflection of the centre mass as a function of the applied impulse. A single curve characterizes the calculated deflections of both the large and small frames. This shows that beam deformations are insensitive to the column member height (within this range). Calculations according to small and large deflection analysis are compared: it is seen that the inclusion of finite deflections does not greatly affect the finite deformation of this type of structure.

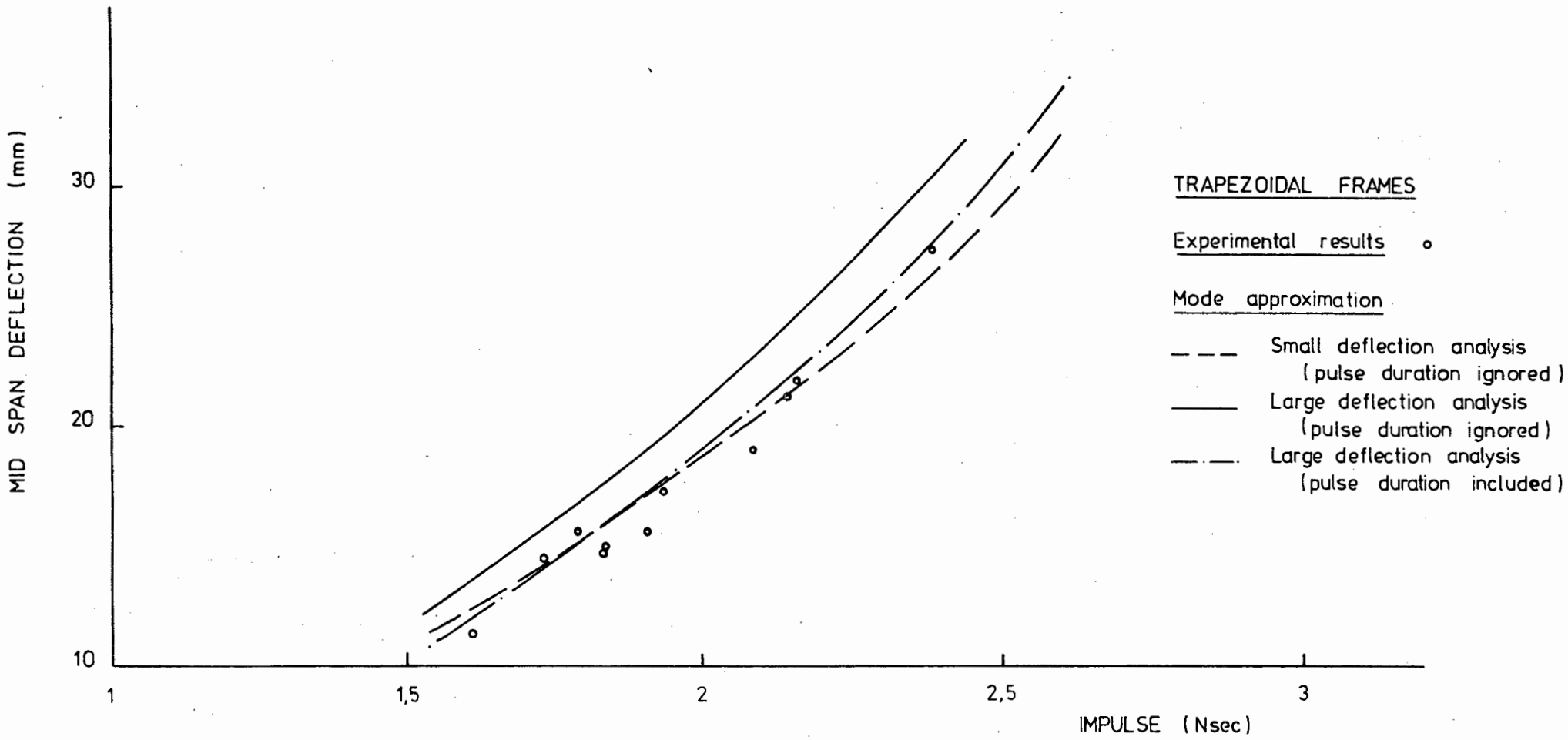

Figure 17 Summary of tests on the trapezoidal frames showing the final deflection of the centre mass as a function of the applied impulse. As would be expected, this kind of structure is more sensitive to finite deformations.

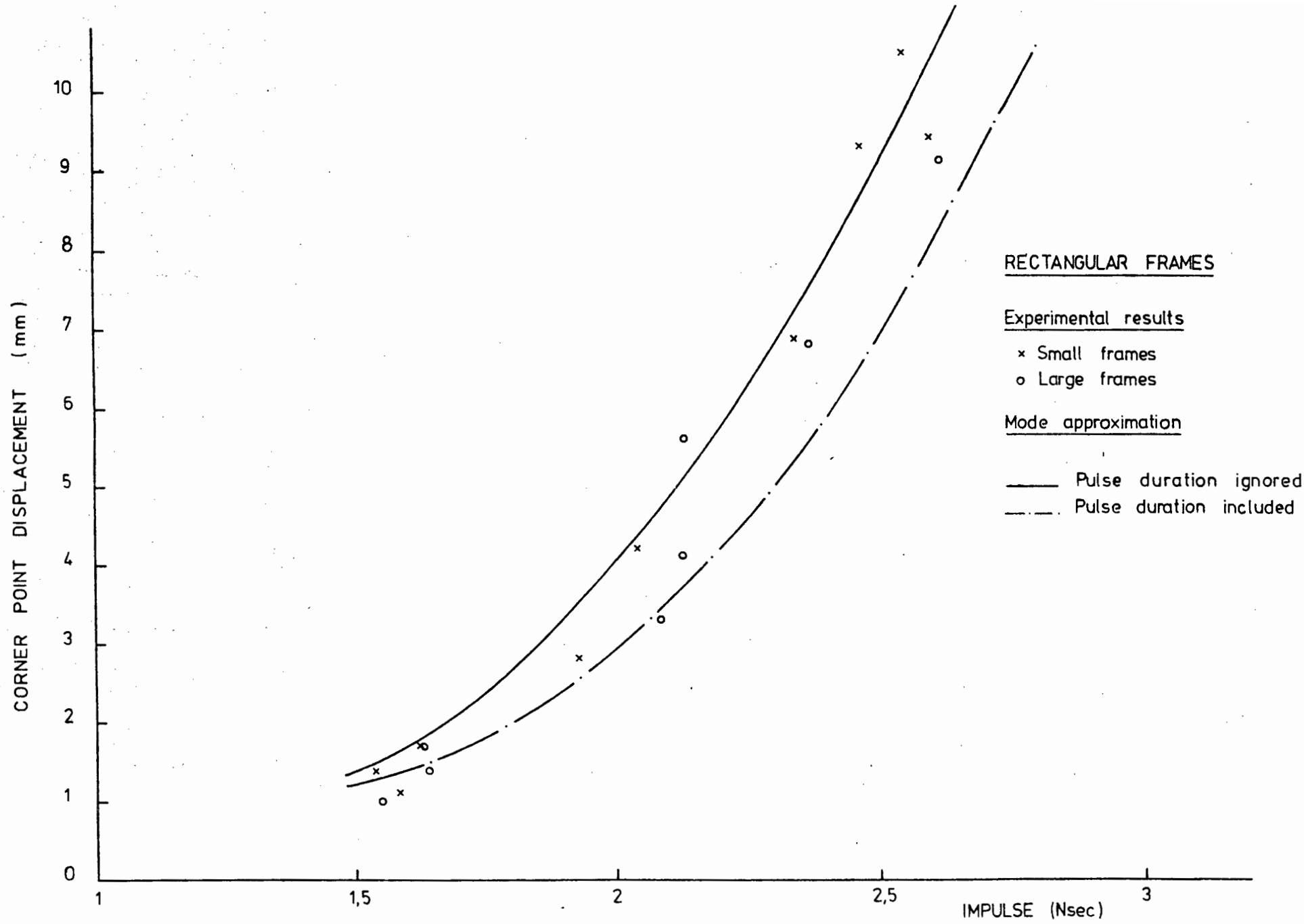

Figure 18 Summary of tests on the rectangular frames showing the final inward displacement at the corner point as a function of the applied impulse. This displacement is zero in the small deflection analysis.

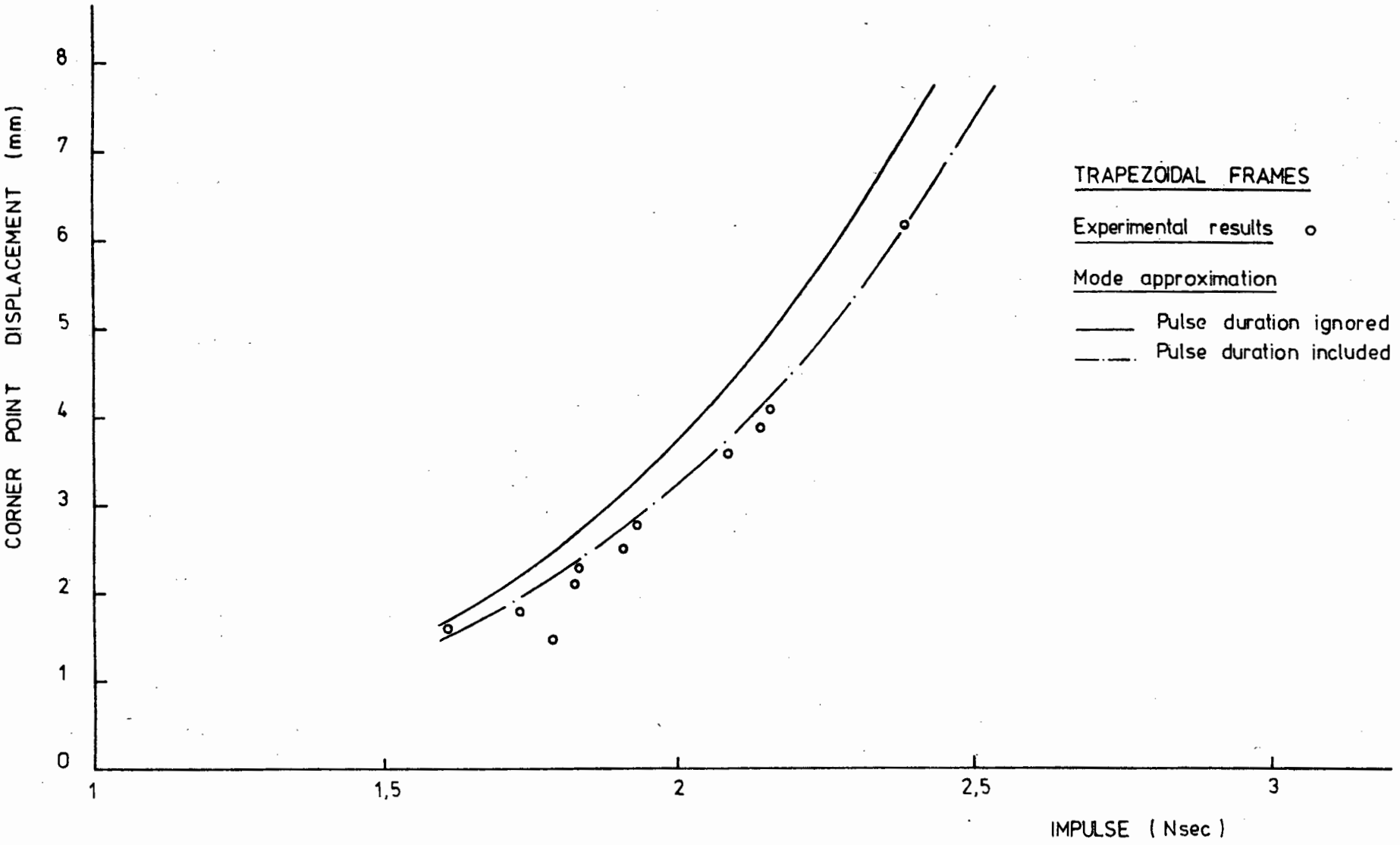

Figure 19 Summary of tests on the trapezoidal frames showing the final inward displacement at the corner point as a function of the applied impulse.

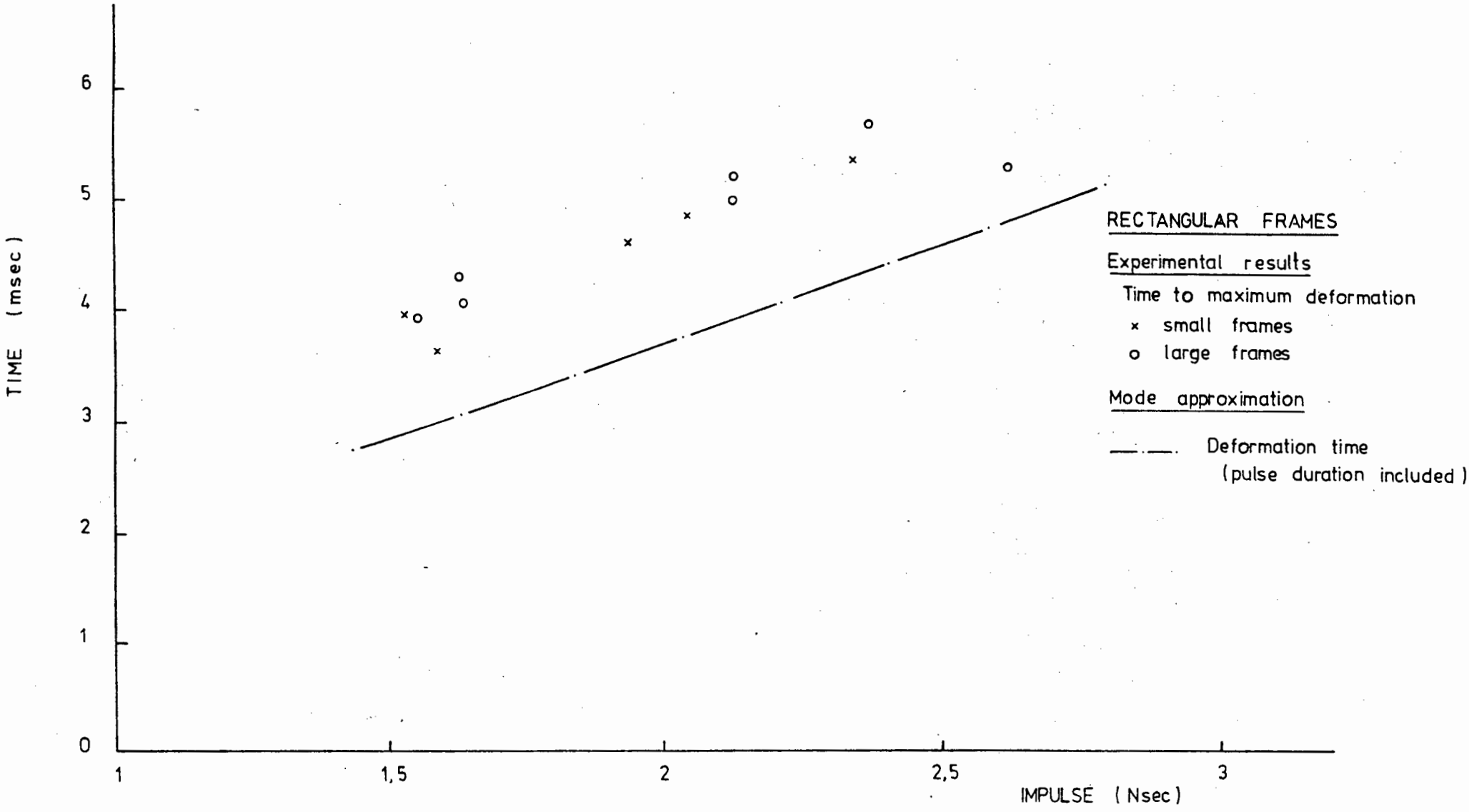

Figure 20 Comparison of observed times to maximum deflection with computed deformation times - trapezoidal frames.

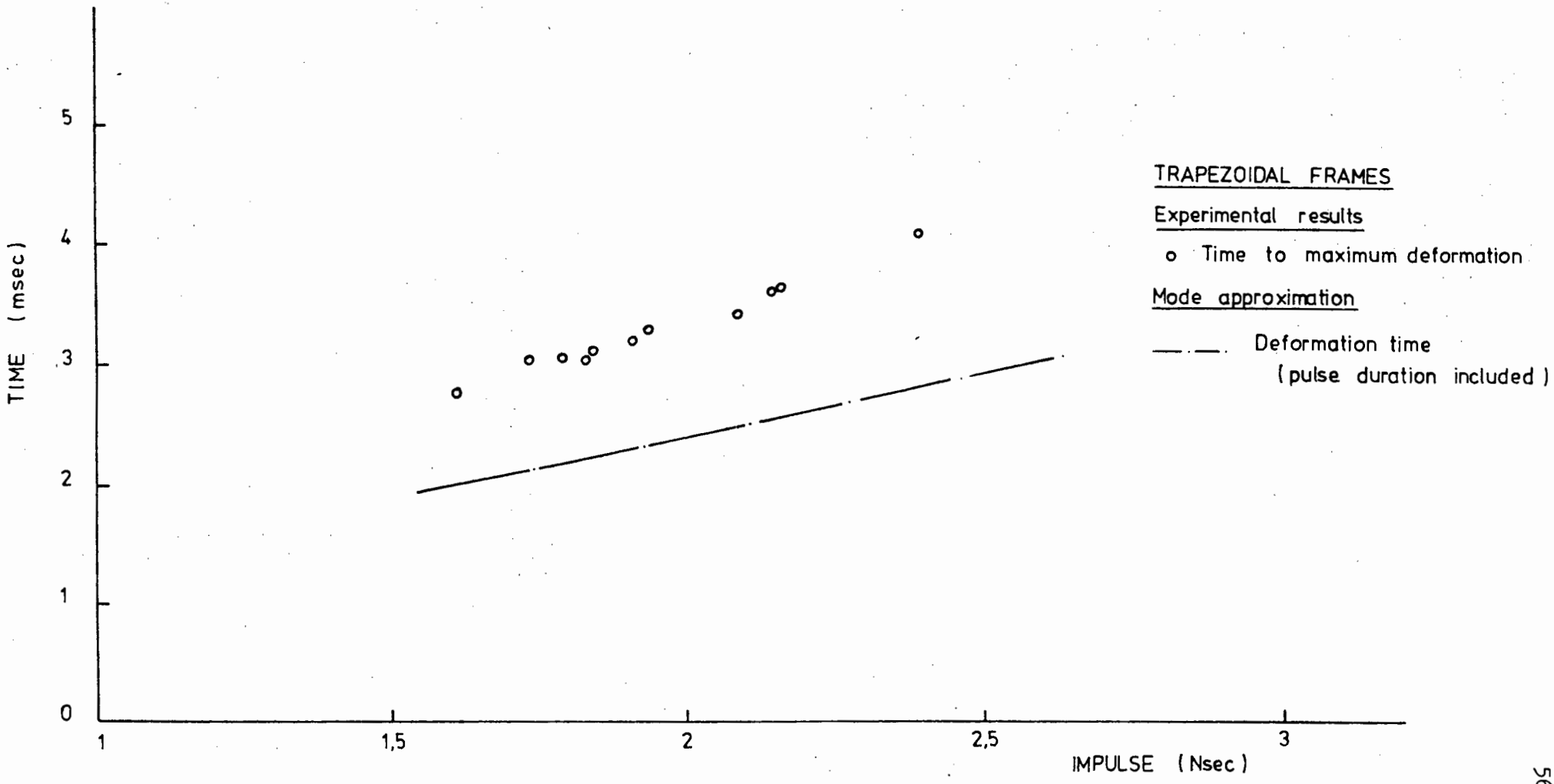

Figure 21 Comparison of observed times to maximum deflection with computed deformation times - trapezoidal frames.

Frame Number	Impulse (N sec)	Pulse duration (m sec)	Energy Ratio **	Mid-span deflection (mm)				Corner point displacement (mm)			Deformation time (m sec)			
				M*	S*	L*	P*	M	L	P	M	S	L	P
SMALL FRAMES														
9	1,538	0,112	4,0	13,1	15,8	16,3	15,3	1,4	1,5	1,3	3,992	2,854	2,972	2,936
11	1,587	0,299	4,3	11,6	16,7	17,3	15,2	1,1	1,7	1,3	3,656	2,937	3,060	3,036
10	1,625	-	4,5	14,8	17,5	18,1	-	1,7	1,8	-	-	3,001	3,128	-
13	1,936	0,523	6,1	20,9	24,5	25,5	21,4	2,8	3,6	2,5	4,626	3,520	3,666	3,662
18	2,045	0,410	6,9	24,7	27,2	28,4	24,8	4,2	4,4	3,3	4,887	3,700	3,847	3,835
1	2,343	0,596	8,7	32,3	35,2	36,9	31,2	6,9	7,2	5,2	5,362	4,188	4,314	4,334
5	2,471	-	9,6	39,0	39,0	40,8	-	9,3	8,7	-	-	4,394	4,500	-
2	2,552	-	10,2	41,8	41,5	43,4	-	10,5	9,7	-	-	4,526	4,615	-
20	2,601	-	10,6	39,4	43,0	45,0	-	9,4	10,4	-	-	4,604	4,681	-

TABLE 2

Summary of experimental and analytical results of the small rectangular frame tests.

* M = experimental
S = mode approximation - small deflection) pulse duration ignored
L = " " - large deflection)
P = " " - large deflection including pulse duration

** The energy ratio is defined in the next section

Frame Number	Impulse (N sec)	Pulse duration (m sec)	Energy Ratio **	Mid-span deflection (mm)				Corner point displacement (mm)			Deformation time (m sec)			
				M*	S*	L*	P*	M	L	P	M	S	L	P
LARGE FRAMES														
8	1,556	0,224	3,4	11,3	16,3	16,7	15,1	1,0	1,6	1,3	3,954	2,914	3,007	2,979
16	1,627	0,299	3,6	13,5	17,7	18,2	16,1	1,7	1,8	1,4	4,335	3,034	3,133	3,111
15	1,643	0,298	3,7	14,4	18,0	18,6	16,4	1,4	1,9	1,5	4,103	3,062	3,162	3,136
21	2,091	-	5,8	25,0	28,6	29,6	-	3,3	4,7	-	-	3,813	3,923	-
6	2,129	0,384	6,0	29,5	29,6	30,7	26,7	5,6	5,1	3,8	5,212	3,876	3,984	3,981
7	2,132	0,460	6,0	25,5	29,7	30,8	27,3	4,1	5,1	4,0	4,982	3,881	3,990	3,976
4	2,371	0,597	7,3	34,6	36,3	37,7	32,1	6,8	7,5	5,5	5,670	4,274	4,359	4,381
14	2,621	0,597	8,7	38,6	44,0	45,7	39,5	9,1	10,7	8,1	5,297	4,683	4,719	4,756

TABLE 3

Summary of experimental and analytical results of the large rectangular frame tests.

Frame Number	Impulse (N sec)	Pulse duration (m sec)	Energy Ratio **	Mid-span deflection (mm)				Corner point displacement (mm)			Deflormation time (m sec)			
				M*	S*	L*	P*	M	L	P	M	S	L	P
11	1,611	0,224	6,4	11,3	12,6	13,7	12,2	1,6	1,7	1,4	2,761	1,938	2,008	2,026
3	1,735	0,224	7,2	14,9	14,5	15,9	14,3	1,8	2,2	1,8	3,059	2,072	2,146	2,166
9	1,789	0,149	7,8	15,5	15,4	16,9	15,9	1,5	2,5	2,2	3,059	2,131	2,205	2,219
6	1,833	0,149	8,1	14,3	16,1	17,8	16,8	2,1	2,7	2,4	3,059	2,179	2,252	2,267
1	1,836	0,297	8,1	14,9	16,1	17,8	15,6	2,3	2,8	2,1	3,122	2,182	2,256	2,285
7	1,907	0,149	8,7	15,5	17,3	19,3	18,3	1,9	3,2	2,8	3,208	2,259	2,331	2,347
12	1,934	0,297	9,0	17,2	17,8	19,9	17,5	2,8	3,4	2,6	3,271	2,288	2,360	2,391
8	2,089	0,224	10,3	19,1	20,7	23,3	21,4	3,6	4,4	3,8	3,432	2,455	2,518	2,546
4	2,146	0,372	10,8	21,1	21,8	24,6	21,2	3,9	4,9	3,7	3,643	2,516	2,575	2,623
10	2,158	0,224	10,9	21,8	22,0	24,9	23,0	4,1	5,0	4,3	3,656	2,528	2,586	2,616
2	2,390	0,223	13,2	27,4	26,7	30,7	28,7	6,2	7,2	6,3	4,103	2,774	2,800	2,838

TABLE 4

Summary of experimental and analytical results of the trapezoidal frame tests.

PART III: DISCUSSION AND CONCLUSION

The comparisons between theoretical calculations and test results are given in the previous section. Figures 9, 10 and 11 compare deflection profiles, while Figures 16 and 17 compare the final deformation of the centre mass. Figures 20 and 21 look at the corner point deflections. Deformation times are given in Figures 20 and 21. It can be seen that in general, the agreement between the mode form solution and the test results is very satisfactory.

The source of possible experimental errors has been discussed in detail in the previous section. Turning to the theory, let us summarize the main approximations made:

i) mode form solution,

ii) viscous constitutive relation,

iii) neglect of strain hardening,

iv) neglect of elastic deformations.

These are all idealizations of conservative type, i.e. they should weaken the structure and deflections should thus be over-estimated. This is generally so, as can be seen in Figures 16 to 19. The calculations are made even more conservative when pulse durations are ignored.

The use of a viscous constitutive law has already been discussed (see also Symonds [7]). The experimental results

which have been obtained over the years do not appear to offer any conclusive evidence concerning the importance of strain hardening [22]. This tends to lend credence to the belief that its influence is rather small. Of more importance is the neglect of elastic deformations. The use of the rigid plastic theory is valid in general when permanent deformations greatly exceed the elastic deformations. A practical rule is that the initial energy should be considerably larger than the maximum amount of elastic strain energy.

The initial kinetic energy may be expressed as

$$\tfrac{1}{2} m\, v_o^2 ,$$

where m is the attached mass, v_o the initial impulsive velocity

The maximum strain energy is estimated as follows: the static collapse mode is assumed, giving the bending moment diagram shown below.

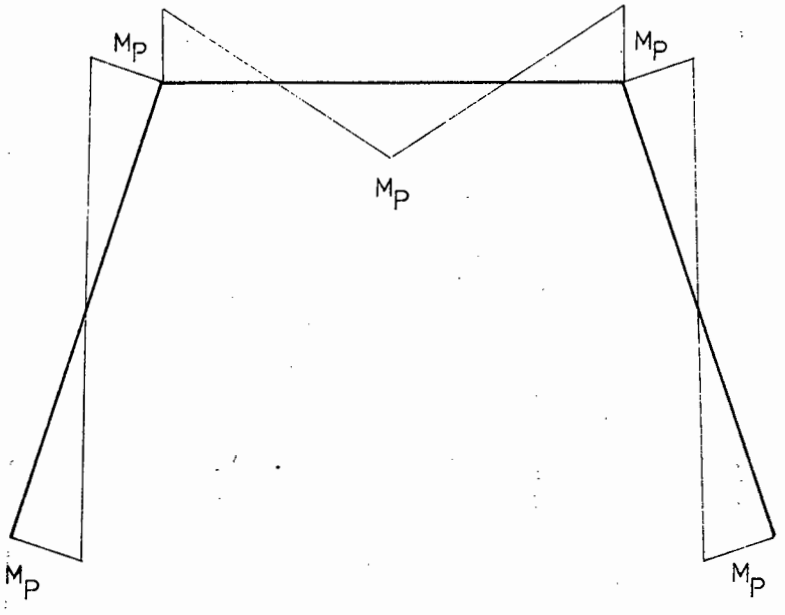

The total strain energy is then

$$E_p = \frac{M_p^2 L}{6EI},$$

where L is the sum of the lengths of the frame members,

EI is the bending stiffness of the members,

M_p is the yield moment given by

$$\frac{M_p}{M_o} = \mu \left(\frac{\dot{\kappa}}{\dot{\kappa}_o}\right)^{\frac{1}{n}},$$

where $\dot{\kappa}$ is the maximum rate of change of curvature determined from the viscoplastic small deflection analysis.

The energy ratio is then given by

$$R_E = \frac{\frac{1}{2}m v_o^2}{\frac{M_p^2 L}{6EI}}$$

The energy ratios for the tests performed are given in Tables 2 and 3 of the previous section. The effect of the energy ratio can be seen by comparing final deformations in rectangular frames and trapezoidal frames. The trapezoidal frames have higher energy ratios and show more consistent results than the rectangular frames (compare Figures 16 and 17 for example). The importance of the elastic deformations is illustrated in Figures 12 to 15 where the transient response of the centre mass is shown. Although, on the average, energy ratios for

these tests are low, the agreement between experiment and theory is good. Symonds and Chon [25] obtained very similar results for low energy ratios. A possible reason for this close agreement is that the elastic deflection in the first phase of the motion is fairly closely compensated by the elastic recovery after the plastic deformation has occurred (see Figures 12 to 15). It is also possible that mutually cancelling errors are occurring. It is clear that at low energy ratios, small factors like unsymmetrical damping (see Figure 12 for example) play an important role in the final deformations. The relative importance of such factors, however decreases as the energy ratio increases and the present method of analysis should become increasingly valid as this ratio increases.

Another factor of importance is the pulse duration. Symonds [12] showed that rigid-plastic analysis predicts meaningful results provided the pulse duration is significantly smaller than the period of natural elastic vibration. The pulse duration in the tests were all small: less than 0,6 msec. Jones [23] showed that for a given value of impulse, there is a small difference between the predictions due to an impulsive velocity (pulse duration ignored) and those due to a rectangular pulse with a peak pressure greater than about five times the corresponding static collapse pressure. This is confirmed here in Figures 16 and 17.

In conclusion, the mode form solution modified to take into account strain rate sensitivity, large deflections and pulse duration provides satisfactory agreement with the results

of tests on steel frames, even at low energy ratios. This technique seems thus promising as an efficient approach to practical problems.

REFERENCES

1. S.J. HASHMI, S.T.S. AL-HASSANI and W. JOHNSON, Large deflection elastic-plastic response of certain structures to impulsive load: numerical solutions and experimental results. Int. J. Mech. Sci., 14, 843, 1972.

2. E.H. WITMER, H.A. BALMER, J.W. LEECH and T.H.H. PIAN, Large plastic deformations of beams,rings, plates and shells. AIAA Jnl., 1, 1848, 1963.

3. J.B. MARTIN and P.S. SYMONDS, Mode approximations for impulsively-loaded rigid-plastic structures. J. Eng. Mech. Div., Am. Soc. Civ. Eng., 92, 43, 1966.

4. P.S. SYMONDS, Viscoplastic behaviour in response of structures to dynamic loading. Proc. Collop. on Behaviour of Metals Under Dynamic Loading, ASME, 1965.

5. L.S.S. LEE and J.B. MARTIN, Approximate solutions of impulsively loaded structures of a rate sensitive material. ZAMP 21, 1011, 1970.

6. L.S.S. LEE, Mode responses of dynamically loaded structures. ASME J. Appl. Mech., 39, 904, 1972.

7. P.S. SYMONDS, Approximation techniques for impulsively loaded structures of rate sensitive plastic behaviour. SIAM J. Appl. Math., 25, 462, 1973.

8. G. AUGUSTI, J.B. MARTIN and J.D. O'KEEFFE, An approximate method of analysis for pulse-loaded rigid-plastic structures. University of Naples, publication 241, 1970.

9. B. RAWLINGS, Impact tests on model steel frames. Proc. Inst. Civ. Eng., 29, 389, 1964.

10. N. PERRONE, Response of rate sensitive frames to impulsive load. ASCE Proc., Eng. Mech. Div. J., 97, 49, 1971.

11. G.L. JOHNSON and J.B. MARTIN, The permanent deformation of a portal frame subjected to a transverse impulse. Int. J. Solids Structures, 5, 1171, 1969.

12. P.S. SYMONDS, Survey of methods of analysis for plastic deformation of structures under dynamic loading. Brown University, Rept. BU/NSRDC/1-67, 1967.

13. M. TAYA and T. MURA, Dynamic plastic behaviour of structures under impact loading investigated by the extended Hamilton's principle. Int. J. Solids Structures, 10, 197, 1974.

14. P. PERZYNA, The constitutive equations for rate sensitive plastic materials. Quart. Appl. Math., 20, 321, 1963.

15. M.J. MANJOINE, Influence of rate of strain and temperature on yield stresses of mild steel. ASME, J. Appl. Mech., 11, A-211, 1944.

16. R.J. ASPDEN and J.D. CAMPBELL, The effect of loading rate on the elastic plastic flexure of steel beams. Proc. Roy. Soc. Am., 290, 266, 1966.

17. J.B. MARTIN, Extremum principles for a class of dynamic rigid-plastic problems. Int. J. Solids Structures, 8, 1185, 1972.

18. P.S. SYMONDS and T. WIERZBICKI, On an extremum principle for mode form solutions in plastic structural dynamics. ASME, J. Appl. Mech., 42, 630, 1975.

19. N. JONES, R.N. GRIFFIN and R.E. VAN DUZER, An experimental study into the dynamic plastic behaviour of wide beams and rectangular plates. Int. J. Mech. Sci., 13, 721, 1971

20. P.S. SYMONDS and N. JONES, Impulsive loading of fully clamped beams with finite plastic deflections and strain-rate sensitivity. Int. J. Mech. Sci, 14, 49, 1972.

21. J.S. HUMPHREYS, Plastic deformation of impulsively loaded straight clamped beams. ASME, J. Appl. Mech, 32, 7, 1965.

22. N. JONES, A literature review of the dynamic plastic response of structures. Shock and Vibration Digest, 7, 8, 1975.

23. N. JONES, A theoretical study of the dynamic plastic behaviour of beams and plates with finite deflections. Int. J. Solids Structures, 7, 1007, 1971.

24. H.E. DAVIS, G.E. TROXELL and C.T. WISKOCIL, The testing and inspection of engineering materials. McGraw Hill, 1964.

25. P.S. SYMONDS and C.T. CHON, Paper to be published

26. W.F. OSGOOD, Mechanics. Dover Publications, Inc.

APPENDIX A

The solution of the differential equation $\frac{d^2}{dx^2} \phi_{xx}^{\frac{1}{n}} = m\Lambda\phi$

This equation is solved using the iterative procedure described in section I.3.

The numerical integration is done in two steps: ϕ_{xx} is first determined and then ϕ using the following integration formulae.

If we define $\psi = \phi_{xx}^{\frac{1}{n}}$, then

$$\psi_1(x_1) = \int_{x_1}^{\ell} (\xi - x_1)\, \psi_{1xx}(\xi) d\xi + a + \frac{G}{2}\Lambda\, (\ell - x_1) \tag{A.1}$$

This takes care of the boundary conditions

$$\psi_{1x}(\ell) = -\frac{G}{2}\Lambda ,$$

$$\psi_1(\ell) = a$$

Also

$$m_1 = -\frac{\delta}{\ell} x_1 + \delta \qquad \text{for } 0 < x_1 < \ell$$

$$m_1 = +\frac{d}{L} x_2 - d + \delta \qquad \text{for } 0 < x_2 < L$$

By the principle of virtual work

$$\int_S m_j \, \phi_{xx} \, dx = 0 \qquad j = 1,2 \tag{A.3}$$

If ψ_1 and ψ_2 are written as (see A.1 and A.2)

$$\psi_1 = f(x_1) + a \,,$$

$$\psi_2 = g(x_2) + a - (L - x_2)b \,,$$

(A.3) becomes

$$-\int_o^L (d - \delta - \frac{d}{L} x_2) \, [g(x_2) + a - (L - x_2)b]^n \, dx_2$$

$$+\int_o^{\ell} \delta(1 - \frac{x_1}{\ell}) \, [f(x_1) + a]^n \, dx_1 = 0 \tag{A.4}$$

$$\int_0^L [g(x_2) + a - (L - x_2)b]^n \, dx_2 + \int_o^{\ell} [f(x_1) + a]^n \, dx_1 = 0 \tag{A.5}$$

We thus have a system of two non-linear equations in two unknowns. a and b may thus be solved using the Newton-Raphson iterative procedure.

ϕ_1 and ϕ_2 may then be obtained using the following formulae:

$$\phi_1(x_1) = \int_o^L x_1 \phi_{2xx}(\xi)d\xi + \int_o^{x_1} (x_1 - \xi)\phi_{1xx}(\xi)d\xi, \quad (A.6)$$

in which the boundary conditions

$$\phi_{2x}(0) = 0 ,$$

$$\phi_1(0) = 0 ,$$

$$\phi_{2x}(L) = \phi_{1x}(0) ,$$

are taken into account.

$$\phi_2(x_2) = \int_o^{x_2} (x_2 - \xi)\ \phi_{2xx}(\xi)d\xi , \quad (A.7)$$

which takes care of the conditions

$$\phi_{2x}(0) = 0 ,$$

$$\phi_2(0) = 0.$$

All of the above integrals may be evaluated using Simpson's quadrature formulae.

APPENDIX B

Computer program: Documentation and listing

1. General specifications

This program was written to analyse steel portal frames. (rectangular or trapezoidal) subjected to an impulse load applied at mid-span of the beam member.

Three different cases are considered:

i) small deflection analysis with pulse duration neglected,

ii) large deflection analysis with pulse duration ignored,

iii) large deflection analysis, including pulse duration

In its present form, the program cannot handle distributed loading. It is further limited to loadings causing deformations symmetrical about the beam centre line. Very minor amendments would be necessary if distributed loading causing symmetrical deformations were considered. Major amendments would be needed in the case of unsymmetrical loading.

The program could also be used for the analysis of frames of any other strain rate sensitive material (e.g. titanium) where the constitutive equation is of the form

$$\frac{M}{M_o} = \mu \left(\frac{\dot{\kappa}}{\dot{\kappa}_o} \right)^{\frac{1}{n}} .$$

2. User specifications

The program is written in FORTRAN V. The execution time is about 7 seconds.

2.1 Input data

The data must be supplied on three cards, in free format

Card 1: IMP,TO,D1,C1.

IMP (Real) : impulse = $\int$Pdt.

TO (R) : pulse duration.

D1 (R) : described below.

C1 (R) : described below.

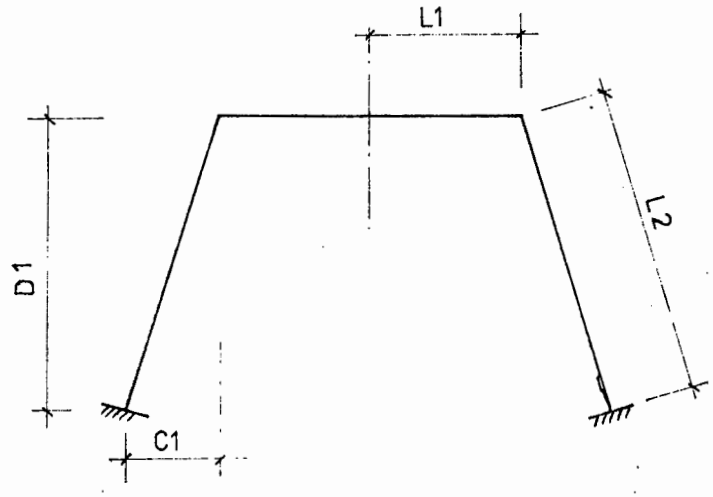

Card 2: L1,L2,M,LOAD,N.

L1 (R) :
L2 (R) : described above

M (R) : mass/unit length of frame

LOAD (R) : mass of centre block

N (R) : value of n in constitutive equation

Card 3: VO,MU,KAPPA,IIFLAG.

VO (R) : instantaneous velocity of centre block.

MU (R) : value of μ in constitutive equation.

MO (R) : static yield moment.

KAPPA (R) : value of $\dot{\kappa}_o$ in constitutive equation.

IIFLAG (Integer) : indicator of the type of analysis required.

Can have 3 values.

1. small deflection analysis, pulse duration ignored,
2. small and large deflection analysis, pulse duration ignored,
3. large deflection analysis, including pulse duration

2.2 Output

A typical output printout is shown in the next page. The deflections given are the deflections of 6 equidistant points of the beam and column members respectively. V1 and U1 refer to the velocity and the deflection of the centre point of the beam member. U2 refers to the corner point displacement.

3. Method

The method has been described in Part I and Appendix A. Only half of the frame is analysed because of symmetry.

SMALL DEFLECTION ANALYSIS
****

RESPONSE TIME	VSTAR
.002182	15.52

DEFLECTIONS

.0000	.0032	.0066	.0101	.0135	.0161
.0000	-.0002	-.0004	-.0006	-.0009	-.0000

LARGE DEFLECTION ANALYSIS
****

TIME	V1	U1	U2
000312	13.10	.0045	.0002
000634	10.72	.0086	.0007
000961	8.39	.0120	.0013
001286	6.12	.0146	.0019
001611	3.92	.0165	.0024
001934	1.83	.0175	.0027
002256	.00	.0178	.0028

DEFLECTIONS

.0012	.0044	.0081	.0118	.0151	.0178
.0000	-.0000	-.0001	-.0001	.0003	.0028

Typical Output Printout

AHA*PULSE(1).FRAME

```
      C                    ******************
      C                    *                *
      C                    *  MAIN PROGRAM  *
      C                    *                *
      C                    ******************
      C
      C
      C  INITIALISE AND DIMENSION THE VARIABLES
      C  ***************************************
            REAL L,L1,L2,LOAD,M,N,MU,MO,KAPPA,LOLO,IMP
            DIMENSION SS(21),W(21),R(21),S(21),T(21),U(21)
            DIMENSION V(21),VV(21),QA(21),RA(21),W(21),Z(21)
            DIMENSION F1(21),F2(21),FXX1(21),FXX2(21),G1(21)
            DIMENSION G11(21),G2(21),G22(21),G(21),F11(21)
            DIMENSION SA(21),SAA(21),TA(21),TAA(21),F(21)
            DIMENSION F1L(21),F2L(21),F1LL(21),F2LL(21),FA1(21)
            DIMENSION DIS1(21),DIS2(21),FIXOLD(21),F2XOLD(21)
            DIMENSION FIX(21),F2X(21),TPRIME(21),FA(21),FB(21)
            READ(8,2000)IMP,TO,C1,D1
            READ(8,2000)L1,L2,M,LOAD,N
            READ(8,2000)VO,MU,MO,KAPPA,IIFLAG
      2000  FORMAT()
      C
            AL1=L1
            AL2=L2
            DELTA1=L1/20.
            DELTA2=L2/20.
            X1=-DELTA1
            X2=-DELTA2
            DO 10 I=1,21
            X1=X1+DELTA1
            F1(I)=-X1*X1/(L1*L1)+2.*X1/L1
            X2=X2+DELTA2
            F2(I)=+(X2**3.)/(2.*L1*L1*L2)-X2*X2/(2.*L1*L1)
      10    CONTINUE
      C
            ICOUNT=1
            C=0.
            D=D1
            A0=0.
            B0=0.
            TIME=0.
            DO 260 I=1,21
            FIXOLD(I)=0.
            F2XOLD(I)=0.
      260   CONTINUE
            L=(L1*(2./(L1*L1))**(1.+1./N)+(N/(2.*N+1.))*L1*L1*L2/3.
           ,*((2./(L1*L1))**(2.+1./N)+(1./(L1*L1))**(2.+1./N)))/
           ,(8.*N*L1/15.+N*L2**5./(420.*(L1**4.))+LOAD/2.)
      C
      C
      C  SOLVE THE DIFFERENTIAL EQUATION
      C  *******************************
      5     DO 20 I=1,21
            PXX1(I)=F1(I)*L*M
            PXX2(I)=F2(I)*L*N
      20    CONTINUE
      C
      C  FIRST INTEGRATION: (1) G(X)
```

```
C  ---------------------------
      DO 30 I=1,20
      X2=(I-1)*DELTA2
      DO 40 J=1,22-I
40    G1(J)=(J-1)*DELTA2*PXX2(I+J-1)
      NP=22-I
      CALL SIMPS(G1,X2,L2,NP,DELTA2,VALUE)
      G11(I)=VALUE
30    CONTINUE
      G11(21)=0.
      DO 50 I=1,21
      X2=(I-1)*DELTA2
      DO 70 JA=1,21
70    G2(JA)=(L2-X2+(JA-1)*DELTA1)*PXX1(JA)
      CALL SIMPS(G2,0.,L1,21,DELTA1,VALUE)
      G22(I)=VALUE
      G(I)=G11(I)+G22(I)+(L2-X2)*LOAD/2.*L+LOAD/2.*L*L1
50    CONTINUE
C
C                        (2) F(X)
C                        --------
      DO 430 I=1,20
      X1=(I-1)*DELTA1
      DO 110 J=1,22-I
      FA1(J)=(J-1)*DELTA1*PXX1(I+J-1)
110   CONTINUE
      NP=22-I
      CALL SIMPS(FA1,X1,L1,NP,DELTA1,VALUE)
      F11(I)=VALUE
      F(I)=F11(I)+(L1-X1)*L*LOAD/2.
430   CONTINUE
      F(21)=0.
C
C  DETERMINE THE CONSTANTS A & B
C  -----------------------------
      AOLD=0.
      BOLD=0.
      IFLAG=0
99    IFLAG=IFLAG+1
      X1=-1.*DELTA1
      X2=-1.*DELTA2
      DDD=DIS1(21)
      DO 140 I=1,21
      SIGNUM=1.
      SIG=1.
      X1=X1+1.*DELTA1
      X2=X2+1.*DELTA2
      Q(I)=G(I)+AO-(L2-X2)*BO
      IF(Q(I).LT.0.)SIGNUM=-1.
      Q(I)=ABS(Q(I))
      IF(Q(I).LT..003)Q(I)=0.
      R(I)=F(I)+AO
      IF(R(I).LT.0.)SIG=-1.
      R(I)=ABS(R(I))
      IF(R(I).LT..003)R(I)=0.
      S(I)=SIGNUM*(D-DDD-D/L2*X2)*Q(I)**N
      SS(I)=SIG*DDD*(1.-X1/L1)*R(I)**N
      T(I)=SIGNUM*Q(I)**N
      U(I)=SIG*R(I)**N
      V(I)=-(D-DDD-D/L2*X2)*N*Q(I)**(N-1.)
```

```
120           VV(I)=DDD*(1.-X1/L1)*N*R(I)**(N-1.)
121           V(I)=-(L2-X2)*V(I)
122           Z(I)=N*Q(I)**(N-1.)
123           QA(I)=N*R(I)**(N-1.)
124           RA(I)=-(L2-X2)*Z(I)
125     140   CONTINUE
126           CALL SIMPS(S,0.,L2,21,DELTA2,A1)
127           CALL SIMPS(SS,0.,L1,21,DELTA1,A2)
128           A=-A1+A2
129           CALL SIMPS(T,0.,L2,21,DELTA2,B1)
130           CALL SIMPS(U,0.,L1,21,DELTA1,B2)
131           B=B1+B2
132           CALL SIMPS(V,0.,L2,21,DELTA2,DADA1)
133           CALL SIMPS(VV,0.,L1,21,DELTA1,DADA2)
134           DADA=DADA1+DADA2
135           CALL SIMPS(W,0.,L2,21,DELTA2,DADB)
136           CALL SIMPS(Z,0.,L2,21,DELTA2,DBDA1)
137           CALL SIMPS(QA,0.,L1,21,DELTA1,DBDA2)
138           DBDA=DBDA1+DBDA2
139           CALL SIMPS(RA,0.,L2,21,DELTA2,DBDB)
140     C
141           AO=AO-((A*DBDB-B*DADB)/(DADA*DBDB-DBDA*DADB))
142           BO=BO-((B*DADA-A*DBDA)/(DADA*DBDB-DBDA*DADB))
143           IF(IFLAG.EQ.250)WRITE(5,2000)A,B
144           IF(IFLAG.EQ.250)GO TO 2
145           IF(ABS(AOLD-A).LT..00001.AND.ABS(BOLD-B).LT..00001)GO TO 7
146           AOLD=A
147           BOLD=B
148           IF(ABS(A).GT..00001.OR.ABS(B).GT..00001)GO TO 99
149     C
150     C  SECOND INTEGRATION: (1) FI2(X)
151     C  ------------------------------
152     7     DO 150 I=2,21
153           X2=(I-1)*DELTA2
154           DO 160 J=1,I
155           SA(J)=(I-J)*DELTA2*T(J)
156     160   CONTINUE
157           CALL SIMPS(SA,0.,X2,I,DELTA2,VALUE)
158           F2(I)=VALUE
159     C
160     C                          (2) FI1(X)
161     C                          ----------
162           X1=(I-1)*DELTA1
163           DO 170 J=1,I
164           SAA(J)=(I-J)*DELTA1*U(J)
165     170   CONTINUE
166           CALL SIMPS(SAA,0.,X1,I,DELTA1,VALUE)
167           TA(I)=VALUE
168           DO 180 J=1,21
169           TAA(J)=X1*T(J)
170     180   CONTINUE
171           CALL SIMPS(TAA,0.,L2,21,DELTA2,VALUE)
172           F1(I)=TA(I)+VALUE
173     150   CONTINUE
174           F2(1)=0.
175           F1(1)=0.
176     C
177     C
178     C  NORMALIZE THE SOLUTION
179     C  **********************
```

```
      ANORM=F1(21)
      DO 190 I=1,21
      F1(I)=F1(I)/ANORM
      F2(I)=F2(I)/ANORM
      IF(ABS(F1(I)).LT.10.E-10)F1(I)=0.
      IF(ABS(F2(I)).LT.10.E-10)F2(I)=0.
190   CONTINUE
C
      DO 210 I=1,21
      U(I)=U(I)/ANORM
      T(I)=T(I)/ANORM
210   CONTINUE
C
C  DETERMINE LAMDA
C  ***************
      DO 200 I=1,21
      F1L(I)=(ABS(U(I)))**((N+1.)/N)
      F2L(I)=(ABS(T(I)))**((N+1.)/N)
      F1LL(I)=F1(I)*F1(I)*M
      F2LL(I)=F2(I)*F2(I)*M
200   CONTINUE
      CALL SIMPS(F1L,0.,L1,21,DELTA1,VALUE1)
      CALL SIMPS(F2L,0.,L2,21,DELTA2,VALUE2)
      CALL SIMPS(F1LL,0.,L1,21,DELTA1,VALUE3)
      CALL SIMPS(F2LL,0.,L2,21,DELTA2,VALUE4)
      LOLD=L
      VAL=VALUE3+VALUE4+LOAD/2.
      L=(VALUE1+VALUE2)/VAL
      IF(ABS(L-LOLD).GT..1)GO TO 5
5000  FORMAT(1H0,X,6F11.4)
C
C
C  SMALL DEFLECTION ANALYSIS SOLUTION
C  **********************************
      IF(ICOUNT.GT.1)GO TO 11
      VISTAR=LOAD*V0/(2.*VAL)
      CONST=(L*MU*M0*VISTAR**(1./3))/(VISTAR*KAPPA**(1./N))
      TF=1./(CONST*(1.-1./N))
      TINT=VISTAR*(N-1.)/(2.*N-1.)*TF
      DO 310 I=1,21
      DIS1(I)=F1(I)*TINT
      DIS2(I)=F2(I)*TINT
310   CONTINUE
      WRITE(5,6000)
6000  FORMAT(1H1,3X,'SMALL DEFLECTION ANALYSIS')
      WRITE(5,15000)
15000 FORMAT(1H ,3X,'**************************')
      WRITE(5,8000)
8000  FORMAT(1H0,//,10X,'RESPONSE TIME',6X,'VSTAR')
      WRITE(5,9000)TF,VISTAR
9000  FORMAT(1H ,12X,F8.6,F12.2)
      WRITE(5,7000)
7000  FORMAT(1H0,//,10X,'DEFLECTIONS')
      WRITE(5,5000)(DIS1(I),I=1,21,4)
      WRITE(5,5000)(DIS2(I),I=1,21,4)
      DO 420 I=1,21
      DIS1(I)=0.
      DIS2(I)=0.
420   CONTINUE
      IF(IIFLAG.EQ.1)GO TO 2
```

```
      WRITE(5,11000)
11000 FORMAT(1H0,/////,5X,'LARGE DEFLECTION ANALYSIS')
      WRITE(5,13000)
      WRITE(5,14000)
14000 FORMAT(1H0,4X,'TIME',5X,'  V1 ',7X,'U1',7X,'U2')
C
C
C
C  DETERMINE THE 1ST DERIVATIVE OF THE MODE SHAPE FUNCTIONS
C  --------------------------------------------------------
11    DO 370 I=2,21
      X2=(I-1)*DELTA2
      CALL SIMPS(T,0.,X2,1,DELTA2,VALUE)
      F2X(I)=VALUE
370   CONTINUE
      F2X(1)=0.
      DO 230 I=1,20
      X1=(I-1)*DELTA1
      NA=0
      DO 240 J=I,21
      NA=NA+1
      TPRIME(NA)=U(J)
240   CONTINUE
      CALL SIMPS(TPRIME,X1,L1,NA,DELTA1,VALUE)
      F1X(I)=-VALUE
230   CONTINUE
      F1X(21)=0.
C
C
C  LARGE DEFLECTION ANALYSIS SOLUTION
C  **********************************
      IF(IIFLAG.EQ.2)GO TO 12
      IF(ICOUNT.NE.1)GO TO 12
      XX=VAL
      YY=(VALUE1+VALUE2)*TO*(N-1.)*MU*RO/(N*KAPPA**(1./N))
18    VO1=VO-(YY*VO**(1./N)+XX*VO-IMP/2.)/
     ,(YY*(1./N)*VO**((1.-N)/N)+XX)
      IF(ABS(VO-VO1).LT.01)GO TO 19
      VO=VO1
      GO TO 18
19    WRITE(5,20001)VO1
      TINT=VO1*(N-1.)*TO/(2.*N-1.)
      TT=TO
      VISTAR=VO1
      GO TO 15
12    CONST=(L*MU*N)*VISTAR**(1./N))/(VISTAR*KAPPA**(1./N))
      TF=1./(CONST*(1.-1./N))
      TT=TF/(8-ICOUNT)
      TINT=VISTAR*TF*(1.-N)/(2.*N-1.)*(1.-TT/TF)**((2.*N-1.)/(1.-N))
      TINT=TINT+VISTAR*(N-1.)/(2.*N-1.)*TF
15    DO 250 I=1,21
      DIS1(I)=DIS1(I)+F1(I)*TINT
      F1X(I)=F1X(I)*TINT
      F1XOLD(I)=F1XOLD(I)+F1X(I)
      FA(I)=(F1XOLD(I)*F1XOLD(I))/2.
250   CONTINUE
      CALL SIMPS(FA,0.,L1,21,DELTA1,ALPHA)
      IF(ICOUNT.EQ.1)AAA=ALPHA*L2/D
      IF(ICOUNT.EQ.1) GO TO 6
      AAA=(ALPHA-C)*(L2/D)/F2(21)
```

```
      6     ICOUNT=ICOUNT+1
            TIME=TIME+TT
      C
      C  DETERMINE THE NEW GEOMETRIC CONFIGURATION
      C  ------------------------------------------
            IF(ICOUNT.GT.2)GO TO 16
            DO 270 I=1,21
            X2=(I-1)*DELTA2
            DIS2(I)=4.*AAA/L2**3.*(X2**4./(12.*L2)
           ,+X2**3./6.)+F2(I)*TINT
            F2X(I)=+4.*AAA/L2**3.*(X2**3./(3.*L2)+X2**2./2.)+F2X(I)*TINT
            FB(I)=(F2X(I)*F2X(I))/2.
      270   CONTINUE
            GO TO 17
      16    DO 410 I=1,21
            DIS2(I)=DIS2(I)+F2(I)*AAA
            F2XOLD(I)=F2XOLD(I)+F2X(I)*AAA
            FB(I)=(F2XOLD(I)*F2XOLD(I))/2.
      410   CONTINUE
      17    CALL SIMPS(FB,0.,L2,21,DELTA2,BETA)
            IF(ICOUNT.NE.2)GO TO 13
            DO 330 I=1,21
            F2(I)=DIS2(I)/TINT
      330   CONTINUE
      C
      C
      13    C=ALPHA
            IF(C1.EQ.0.)D=D1-BETA
            IF(C1.NE.0.)D=D1-BETA*D/L2
            L1=AL1-C
            L2=AL2-BETA
            DELTA1=L1/20.
            DELTA2=L2/20.
            D21=DIS1(21)+BETA*D/L2+C*C1/D
            IF(IIFLAG.EQ.3.AND.ICOUNT.LT.3)GO TO 31
            IF(ICOUNT.LT.3)VISTAR=VISTAR*(1.-TT/TF)**(N/(N-1.))
            IF(ICOUNT.EQ.4)VISTAR=0.
      31    WRITE(5,12000)TIME,VISTAR,D21,DIS2(21)
      12000 FORMAT(1H ,F8.6,3X,F7.2,3X,F8.4,3X,F6.4)
            IF(ICOUNT.LT.3)GO TO 5
            DO 440 I=1,21
            DIS1(I)=DIS1(I)+BETA*D/L2+C*C1/D
      440   CONTINUE
            WRITE(5,7000)
            WRITE(5,5000)(DIS1(I),I=1,21,4)
            WRITE(5,5000)(DIS2(I),I=1,21,4)
      2     STOP
            END
```

DANA*PULSE(1).SIMPS

```
      1       C  NUMERICAL INTEGRATION BY SIMPSON'S RULE
      2       C  **********.**********.**********.**********
      3       C
      4             SUBROUTINE SIMPS(AX,XA,XB,NP,STEP,VALUE)
      5             DIMENSION AX(101)
      6             IF(NP.EQ.2)VALUE=(AX(1)+AX(2))*(XB-XA)/2.
      7             IF(NP.EQ.2)GO TO 2
      8             NP1=NP/2
      9             NP2=2*NP1
     10             IF(NP.NE.NP2)GO TO 1
     11             VALUE=3.*STEP/8.*(AX(1)+3.*AX(2)+3.*AX(3)+AX(4))
     12             IF(NP.EQ.4)GO TO 2
     13             S1=0.
     14             S2=0.
     15             IF(NP.EQ.6)S1=AX(5)
     16             IF(NP.EQ.6)GO TO 4
     17             DO 30 I=5,NP-1,2
     18       30    S1=S1+AX(I)
     19             DO 40 I=6,NP-2,2
     20       40    S2=S2+AX(I)
     21       4     VALUE=VALUE+(AX(4)+AX(NP)+4.*S1+2.*S2)*STEP/3.
     22             GO TO 2
     23       1     S1=0.
     24             S2=0.
     25             IF(NP.EQ.3)S1=AX(2)
     26             IF(NP.EQ.3)GO TO 3
     27             DO 10 I=2,NP-1,2
     28       10    S1=S1+AX(I)
     29             DO 20 I=3,NP-2,2
     30       20    S2=S2+AX(I)
     31       3     VALUE=STEP/3.*(AX(1)+AX(NP)+4.*S1+2.*S2)
     32       2     RETURN
     33             END
```